Toward Optogenetic Control of Neural Synchrony: Experimental
Results from the Hippocampal Slice Model of Gamma Oscillations and
Computational Modeling

by

Giovanni Talei Franzesi

B.S. in Mechanical Engineering-Biomedical Engineering Track
Massachusetts Institute of Technology, 2006

M. Eng. in Biomedical Engineering
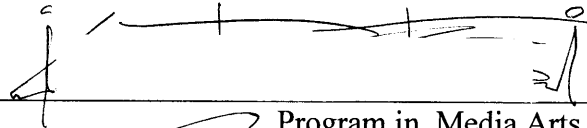Harvard-MIT Division of Health Sciences and Technology, 2008

Submitted to the Program in Media Arts and Sciences, School of Architecture and Planning in
partial fulfillment of the requirements for the degree of

MASTER OF SCIENCE IN MEDIA ARTS AND SCIENCES

September 2009

Signature of Author_____
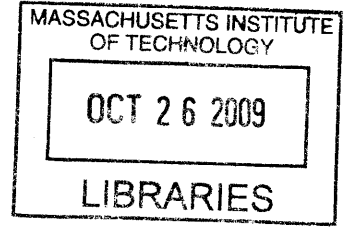Program in Media Arts and Sciences
August 7th, 2009

Certified by_____
Edward S. Boyden, III
Benesse Career Development Professor

Accepted by_____
Prof. Deb Roy
Chair, Departmental Committee
on Graduate Students

Toward Optogenetic Control of Neural Synchrony: Experimental

Results from the Hippocampal Slice Model of Gamma Oscillations and

Computational Modeling

by

Giovanni Talei Franzesi

Submitted to the Program in Media Arts and Sciences, School of Architecture and Planning on

August 7, 2009 in partial fulfillment of the requirements for the degree of

MASTER OF SCIENCE IN MEDIA ARTS AND SCIENCES

ABSTRACT

Ever since Hans Berger recorded the first human EEGs in humans and observed large, rhythmic 8 Hz field oscillations, neuroscientists have been intrigued by the pervasive presence of synchronized, regular patterns of the activity in the brain. A number of frequency bands, spanning from 0.1 to several hundred hertz have been described, and associated with particular functions and brain states. Not surprisingly, disruptions in such patterns have been postulated to be the mechanistic basis of a number of disorders, from schizophrenia to Parkinson's disease, to Alzheimer. Until now, however, virtually all evidence on the role of synchronous oscillations in brain functions has been merely correlative, that is, it has never been possible to selectively manipulate neural synchrony without altering other fundamental properties of the system and observing the functional outcome.

This limit may now be overcome with the introduction of genetically targeted light-activeatable means of controlling neural activity, which allows spatially and temporally precise control of the activity of determined classes of neurons. Although the ultimate goal is to observe the functional, behavioral outcomes of modulating synchrony in awake animals, it's necessary first to develop such techniques in vitro, if we are to be able (given the current technological limitations) to extract useful "design principles" that can meaningfully generalize. A particularly well-studied, reliable and yet relevant in vitro model, is the hippocampal slice gamma oscillations model, so we have been focusing on those as a testbed, integrating experimental work with computational modeling.

Among the previously undescribed capabilities we have gained in the process are: precisely resetting the phase of an ongoing gamma oscillation, altering its frequency, and modulating its amplitude.

Edward S. Boyden, III
Benesse Career Development Professor

ACKNOWLEDGEMENTS

:

Reader _____

Nancy Kopell

Co-director, Center for BioDynamics

Professor, Boston University Department of Mathematics

Reader _____,

Robert Desimone

Director, McGovern Institute;

The Doris and Don Berkey Professor of Neuroscience

4

Table of Contents

1. Introduction

Over the past two centuries, the engineering disciplines have played key roles toward the advancement of human condition. In a schematic (and much simplified) progression, first mechanical engineering allowed the control of the physical world to degrees hitherto imagined, then electrical engineering opened the doors to the current digital age, which has in many ways made spatial distance irrelevant, and now biomedical engineering holds great promise to preserve and potentially even enhance the human body. Similarly, the emerging new discipline of neuroengineering s can be defined as a conceptual and practical framework to understand and engineer neural circuits to address psychiatric disorders and augment cognition.

Of fundamental importance along this pursuit is to define what a suitable scale for investigation and manipulation is. Although there are several meaningful lengthscales, one could broadly consider overall regions as the macroscale, cell-population level dynamics as the mesoscale, and the individual cell, synapse, spike, as the microscale. Of these, the first is what has been clinically used so far, using either surgical ablation or functional "shutdown" (e.g. with DBS), while the third is still far beyond our capabilities, and may ultimately prove unnecessary, in light of the redundancy and robustness typically built in biological systems. In contrast, we are starting to develop both experimental methods and conceptual frameworks to start understanding and manipulating the brain at what we called the "intermediate" scale.

Ever since Hans Berger recorded the first human EEGs in humans and observed large, rhythmic 8 Hz field oscillations, neuroscientists have been intrigued by the pervasive presence of synchronized, regular patterns of the activity in the brain. A number of frequency bands, spanning from 0.1 to several hundred hertz (Bragin et al., 1999, Buzsaki and Draguhn, 2004) have been described, and associated with particular functions and brain states. Not surprisingly, disruptions in such patterns have been postulated to be the mechanistic basis of a number of disorders, from schizophrenia to Parkinson's disease, to Alzheimer(Uhlhaas, Linden et al. 2006). Among the most frequently studied of such frequency bands is the gamma band (30-80 Hz) which has been implicated in cognitive, attentional and perceptual behaviors, both in humans and in laboratory animals(Womelsdorf et al., 2006, Womelsdorf et al., 2007, Fries et al., 2007, Fries

et al., 2001, Fries et al., 1997). Among the functions of temporal synchrony in this band that evidence suggests are the binding of sensory features into a gestalt, (Gray, Konig et al. 1989; Singer 1999) and, more generally, the formation of meaningful cell assemblies(Borgers, Epstein et al. 2005; Tort, Rotstein et al. 2007; Borgers, Epstein et al. 2008). Gamma-band synchrony has also been postulated to be crucial for the efficient coding and transmission of information, in cooperation with other frequency bands (Fries, Nikolic et al. 2007) (Kopell, Ermentrout et al. 2000; Jensen, Kaiser et al. 2007).

Intriguingly, alterations in gamma synchrony have been described in human schizophrenic patients as well as in animal models of the disease(Uhlhaas et al., 2006, Basar-Eroglu et al., 2007, Light et al., 2006, Lisman and Buzsaki, 2008, Spencer et al., 2008, Uhlhaas and Singer, 2006, Wilson et al., 2008, Roopun et al., 2008) and could indeed be of fundamental importance in the pathophysiology of this disorder if its postulated roles in normal brain functions are indeed correct. Thus, in addition to its intrinsic value in terms of basic neuroscience, gaining a better understanding of the biophysical origins of such synchrony, and the development of techniques for selectively altering it could be of great therapeutic interest, for addressing one of the most devastating human diseases.

Until now, however, virtually all evidence on the role of synchronous oscillations in brain functions has been merely correlative, that is, it has never been possible to selectively manipulate neural synchrony without altering other fundamental properties of the system and observing the functional outcome. This limit may now be overcome with the introduction of genetically targeted light-activeatable means of controlling neural activity, which allows spatially and temporally precise control of the activity of determined classes of neurons.

Although the ultimate goal is to observe the functional, behavioral outcomes of modulating synchrony in awake animals, it's necessary first to develop such techniques in vitro, if we are to be able (given the current technological limitations) to extract useful "design principles" that can meaningfully generalize. A particularly well-studied, reliable and yet relevant in vitro model are the hippocampal and neocortical slice gamma oscillations models, so we have been focusing on those as a testbed.

At the same time, if we want to move beyond a simple description of the brain to something more akin to true neural engineering, we need models, to make sense of our observations and predict the response of the network studied to novel perturbations, so part of the effort is being devoted to validating and integrating existing, biophysically realistic models of neural rhythmogenesis.

We are focusing on relatively simple "minimal network" models, because they are computationally tractable and allow considerable intuitive insight, while at the same time capturing some important aspects of the system under study.

2. Optogenetic methods for the control of neural activity

One of the major limitations in neuroscience during the last century was the inability to manipulate neuronal activity with a high degree of temporal and cell-type selectivity. Electrical stimulation allows exquisite temporal precision, but acts indiscriminately an all nearby cells (albeit to different degrees); conversely, pharmacological manipulations, both systemic and local offer greater specificity, but suffer from slow timescales of onset-offset.

Over the last few years, we and others have adapted a set of naturally-occurring microbial opsins for neural expression, thus allowing specific genetically-defined neuron types expressing these opsins to be activated and silenced by pulses of light in a temporally-precise fashion. These microbial opsins are 7-transmembrane proteins that bind the cofactor all-trans-retinal, which naturally occurs in the mammalian brain, obviating the need for ad-hoc supplementation with exogenous chemicals.
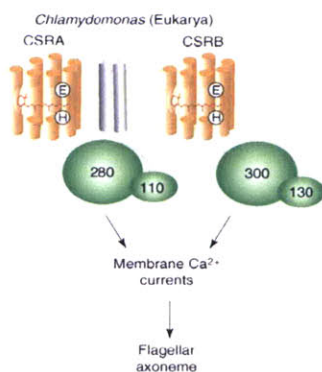
Figure 1: structure of light-activated ion pump Channelrhodopsin-2 (Chr-2) (Litvin, Sineshchekov et al. 1978)

The first channel to be used in this fashion was the light-gated cation channel channelrhodopsin-2 (ChR2)(Boyden, Zhang et al. 2005) from the alga *C. reinhardtii*. Following transfection or viral infection (Figure 1A),cultured hippocampal neurons experience strong depolarizing currents in response to blue (~450-490 nm) light (Figure 1B), allowing reliable spike firing in response to brief (1-10 ms duration) pulses of blue light at light powers of 1-10 mW/mm2. To complement this optical method for neuronal stimulation our group first described (Han and Boyden 2007) the use of a light-driven chloride pump halorhodopsin (Halo/NpHR) from the archaebacterum *N. pharaonis* to induce hyperpolarizing currents in response to yellow (~570-610 nm) light (Figure 1E), allowing spike silencing in response to pulses of yellow light (Figure 1F) (figure adapted from (Han and Boyden, 2007)).
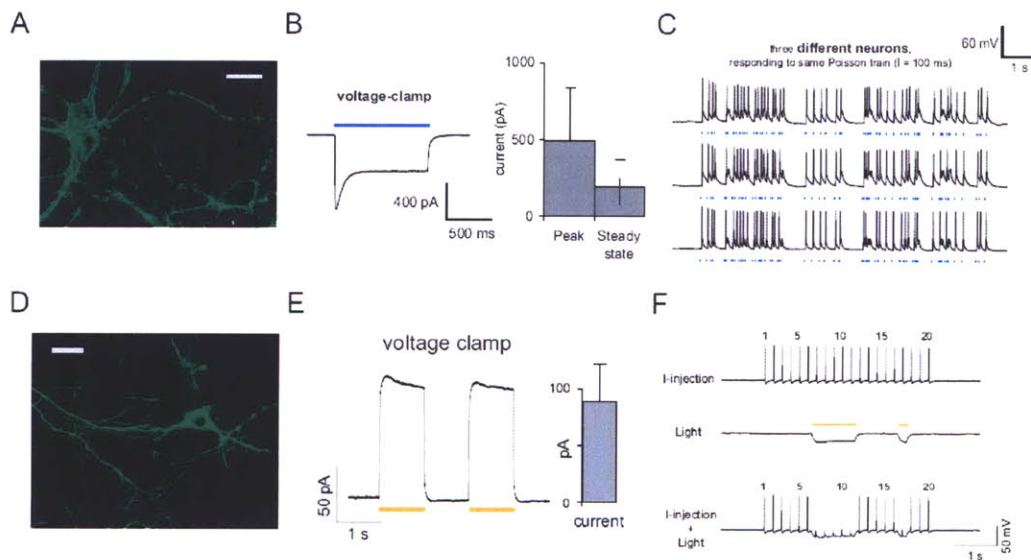
Figure 2: A,B,C: fluorescence micrograph and electrophysiogical recordings from cultured hippocampal neurons expressing Chr2. D,E,F fluorescence micrograph and electrophysiogical recordings from cultured hippocampal neurons expressing the light-activated chloride pump Halorhodopsin (Han and Boyden 2007).

Importantly, the two opsins can be driven by sufficiently different wavelengths so that both can be used, either in two cell populations or even to bidirectionally modulate the same cell. In the latter case, to ensure exact stochiometric expression of the two opsins, a promising approach seems to be the use of a linker construct, such as the picornavirus-derived 2A construct (Furler, Paterna et al. 2001) (Quiang, Han et al. 2008).
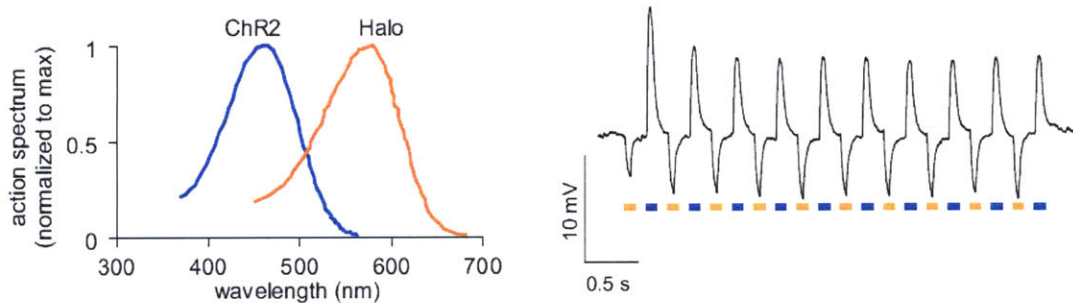
Figure 3. Chr2 and Halorhodopsin spectral responses only partially overlap (A), allowing their simultaneous use in the same cell (B)(Han and Boyden 2007).

Over the past two years, substantial advances have been made in the discovery, modification and application of light-sensitive ion channels and pumps for neuroscience applications. For example, halorhodopsin currents benefit by ~75% from sequences that improve trafficking to the membrane (Gradinaru et al., 2008; Zhao et al., 2008), while newer opsins (Chow et al. 2009) allow still-improved neural silencing. Recently, opsins have also been developed or discovered that mediate improved optical activation at high frequencies (Lin, Lin et al. 2009; Wang, Sugiyama et al. 2009) and that respond to other wavelengths of light(Zhang, Prigge et al. 2008) .

In conjunction with better opsins, the methods employed to deliver light have also seen constant improvements, leading to the ability to multi-color control of several different brain regions, coupled with electrical recordings (Bernstein, Han et al. 2008)

In addition to improved temporal and spatial resolution, optogenetic methods allow for the first time the targeting of specific cell classes. This has been so far pursued with a number of strategies. Despite intensive efforts, the development of transgenic mice has so far yielded only two published channelrhodopsin-2 expressing lines to date, in which ChR2 is expressed under the Thy1 promoter (Wang, Peca et al. 2007), and these lines express ChR2 within excitatory

neurons in layer 5 of cortex, excitatory neurons of hippocampus, and subsets of cells in other areas.

More commonly, strategies have been employed to deliver the gene of interest, under the control of a cell-type specific promoter, to the cells of wild-type animals. Electroporation and gene-gunning are two strategies that have enabled plasmids containing ChR2 behind a cell-specific promoter to be used to express ChR2 in specific cell types of the retina, hippocampus, and cortex(Petreanu, Huber et al. 2007; Zhang and Oertner 2007; Lagali, Balya et al. 2008). Similarly, lentiviruses carrying an opsin under a cell-specific promoter have also been used to permanently integrate the opsin gene into the cell's genome, a fairly general strategy that works with multiple different promoters, in species from mouse to non-human primate(Boyden, Zhang et al. 2005) (Nagel, Brauner et al. 2005; Schroll, Riemensperger et al. 2006; Adamantidis, Zhang et al. 2007; Zhang, Aravanis et al. 2007; Han, Qian et al. 2009)

Another strategy emerges from the fact that Cre recombinase will bind to pairs of lox sites and induce genetic recombination between the sites(Kuhlman and Huang 2008). Since many mice exist that express Cre recombinase in specific cell types (serotonin-generating neurons, dopamine-generating neurons, Parvalbumin-expressing neurons, etc. – many available from Jackson Labs or other sources), using an AAV containing an opsin either behind a lox-flanked transcriptional stop sequence or embedded in an inverted fashion surrounded by different sets of lox sites (Atasoy, Aponte et al. 2008)be used to achieve cell-type specific expression of opsins, simply by injecting the virus into the appropriate cell type-specific Cre mouse (Figure 4B).
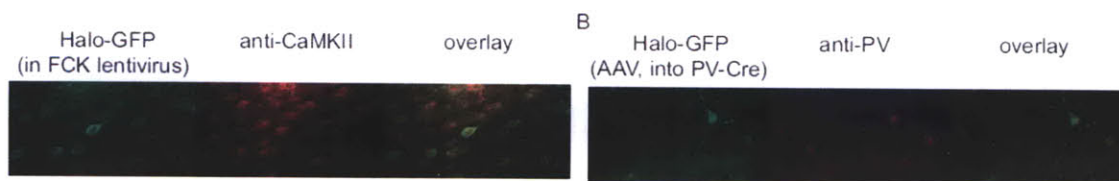
Figure 4. A. Fluorescent micrographs of tissue samples double-stained with anti-GFP and anti-CamkII antibodies, demonstrating the cell-type specificity of Halo-GFP carried in a lentiviral vector(Han, Qian et al. 2009). B. Fluorescent micrographs of tissue samples double-stained with anti-GFP and anti-PV antibodies demonstrating the specificyt of GFP-halo expression with a AAV-loxP-stop-loxP X PV-Cre transgenic approach

3. Developments of electrodes compatible with optical stimulation

A major advantage of the use of optogenetic technologies would be allowing simultaneous recording and stimulation (Bernstein, Han et al. 2008), which has so far proved impractical with electrical stimulation.

However, it is well known (see (Gratzel 2001; Honda 2004) for review) that metal or semiconducting electrodes in a solution can generate a photocurrent upon illumination. Early experimentation confirmed that in fact commonly used metal or silicon electrodes (Figure 1) would in fact show a light-induced artifact (Han, Qian et al. 2009) at both stimulus onset and offset. While the relatively long time constant of the effect allowed the recording of spikes from stimulated cells, it prevented the successful recording of local field potentials. Given the fact that synchronous activity is normally observed in the local field potentials and in spike-field coherence this was a substantial limitation, which we aimed to address with the introduction of "light-proof" electrodes.
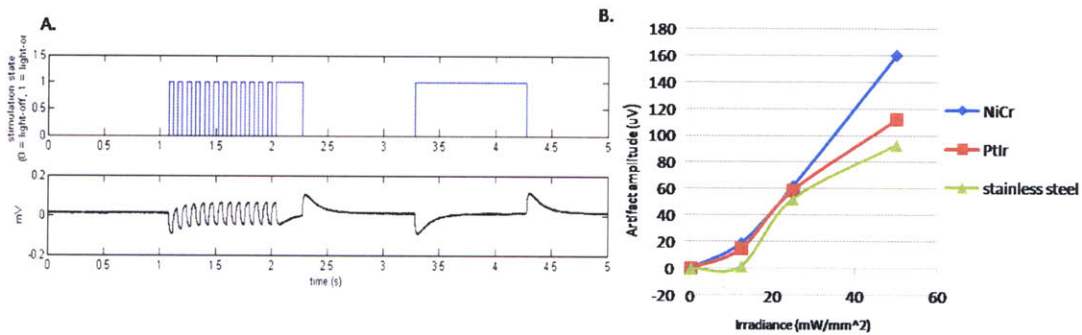
Figure 1. Average of 10 traces recorded in saline with a 25 μm NiCr wire microelectrode (impedance of 1.2 MΩ), illuminated at 50mW/mm^2. B. artifact size (μV) vs. irradiance (mW/mm^2) for PtIr, NiCr, stainless steel electrodes.

The conversion of light to electrical or chemical (redox) energy, and hence the measured photocurrent, results from light acting as an electron pump. The absorption of a photon by an atom or molecule pumps an electron from a lower orbital to a higher one, giving rise to an electron-hole (e- h+) pair: if the electron is then pumped through a wire a current has been generated. The wavelength of light that causes such a transition is that with energy equal to or greater than the difference in energies of the two orbitals. Importantly, for metal electrodes, the difference between the work function E_f of electrode metal and solvation energy of electrons E_{solv}

14

corresponds to the photoenergy required for generating photocurrent, which is much lower to what would be in vacuum.

The mechanism behind the generation of a photocurrent (photogalvanic effect) in a semiconductor is similar. When a semiconductor is placed in contact with an electrolyte, electric current initially flows across the junction until electronic equilibrium is reached, where the Fermi energy of the electrons in the solid (EF) is equal to the redox potential of the electrolyte (E_{redox}: the transfer of electric charge produces a region on each side of the junction where the charge distribution differs from the bulk material, and this is known as the space-charge layer. Photons of energy exceeding that of the band gap generate electron–hole pairs, which are separated by the electric field present in the space-charge layer. The negative charge carriers move through the bulk of the semiconductor to the current collector and the external circuit. The positive holes are driven to the surface where they are scavenged by the reduced form of the redox relay molecule (Gratzel 2001; Honda 2004)

Because the exact details of the galvanic effect depends upon the specific surface and electrolyte chemistry and light characteristics at each electrode/solution interface, all highly variable in the case of electrode used in a physiological milieu, a filtering operation, correcting in software for the artifact is impractical. The approach we chose, instead, relies on employing a conducting material that has a large enough bandgap to be only marginally affected by visible light (since $E_{photon} = \lambda v$): among commonly used materials employed for bioengineering applications Indium Tin Oxide (ITO) appeared the most promising candidate satisfying this requirement.

Although Michigan-style probes have gained popularity, microwire electrodes are still used and preferred for many applications: they are much cheaper, simple to use, generally induce less tissue damage, and, in the case of tetrodes, allow much better single-unit separation. Since the metals in vacuum are not much affected by light, we postulated that if we could "shield" them with a layer of ITO, which would be the only conductive material in contact with the surrounding fluid, we should get a substantial reduction, if not a complete elimination, of the artifact.

The fabrication technique had to be scalable, cheap, simple and biocompatible. The procedure we have developed is schematically illustrated in Figure 2. Briefly, the wires or tetrodes bundles were placed on a frame, then a holder was cast around the wires in machinable wax, or PMMA resist, ensuring perfect contact. The wires were then trimmed, etched and the ITO was deposited by RF sputtering. Sputtering was chosen because it's a simple, scalable technique which allows very mild conditions and doesn't involve biologically hazardous materials.
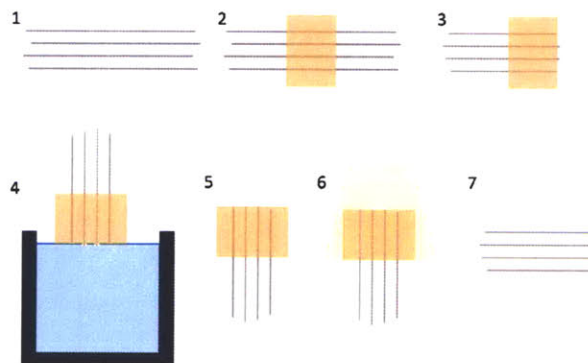

Figure 3. Schematic of the fabrication procedure for ITO-coated microwire electrodes. 1. The wires are attached to a frame. 2. Molten machinable wax (McMaster Carr, softening point 240 F, hardness 51 D) is poured in the mold, embedding the wires. 3 The wires are trimmed and the block is released from the mold. The wires are further trimmed up to approximately the surface of the wax. 4, 5. the construct is then dipped in an acid bath that affects the selective removal of the metal, without affecting either the wax holder or the insulation around the wires. This is important to ensure that only a "face" of wire is coated with ITO. 6. ITO is then deposited by RF sputtering, in order to ensure a uniform coating the thingamajig is rotated a few times. 7. The wax is then molten to liberate the wires.

An alternative that we did explore was to use ITO nanoparticles suspension: the electrode would be dipped, the ITO layer sintered at 300-500° C, and the process repeated until an ITO layer of the desired thickness was achieved. This method recommended itself because of its low cost, and because it gives a corrugated surface (Fig. 3), which tends to decrease impedance, in a manner similar to platinum black. However, this technique tends to be very time consuming and less reliable than the sputtering method, so was eventually abandoned. At the same time, sintering ITO nanoparticles on top of a sputtered substrate may be a useful approach to further decrease the electrode impedance, if needed.
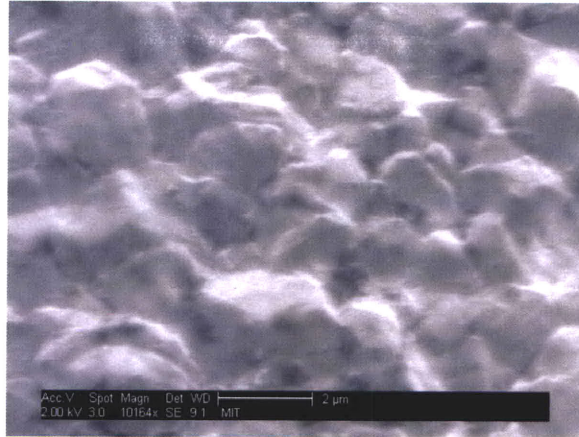
Figure 3. SEM microgram of a tungsten microelectrode coated by repeated dipping in an ITO nanoparticles solution followed by sintering at 400^{0}C

The microwire electrodes thus obtained did in fact show a remarkable decrease in the photogalvanic effect (Figure 4), the amplitude of the artifact being reduce over 20-fold over the uncoated wires. At the same time, the impedance remained within reasonable values (1-3 MΩ).
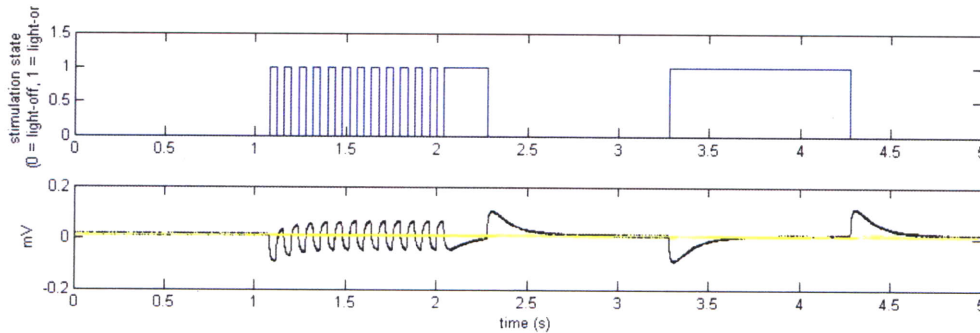
Fig. 4 Average of 10 recordings from NiCr electrodes in saline, before (black) and after (yellow) ITO deposition (bottome trace). The top trace indicates the times of stimulation.

Despite the qualities of microwire electrodes, multielectrode probes have also proved extremely useful (Buzsaki 2004; Kipke, Shain et al. 2008): by having a number of electrodes aligned at a given distance from each other, not only it's possible to accrue a large mass of data with relatively limited tissue damage, but this configuration is also perfectly suited to analyzing layered structures (such as the neocortex or the hippocampus), and allows CSD computations.

However, conventional probes are also subject to the photoelectric effect: we therefore developed ITO-on glass probes (Figure 6 A,B) that can be fabricated with standard photolithographic method, allow multiple-site recordings, and are light-insensitive.
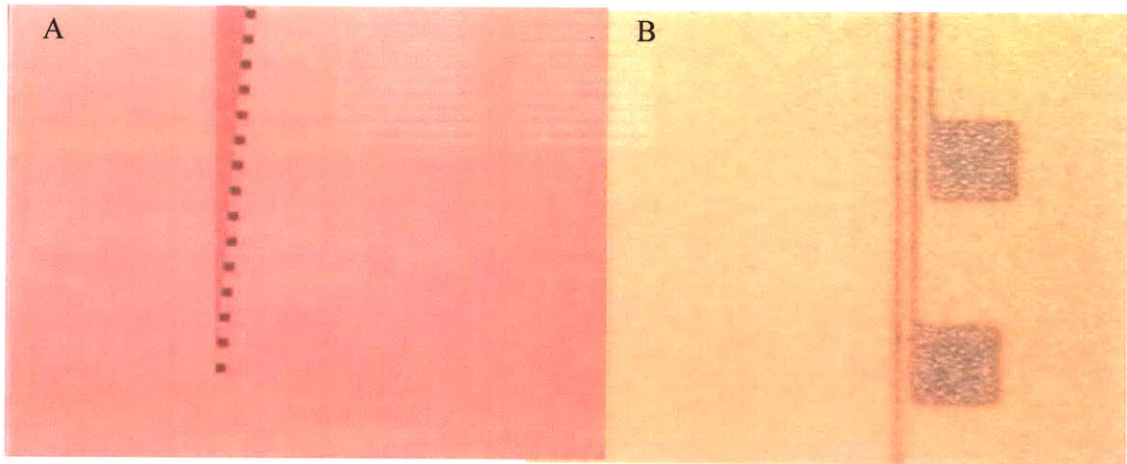
Figure 6. micrographs of the glass-on-ITO probe, showing the recording sites. 5x (A) and 40x(B). Courtesy of Anthony Zorzos, MS

Overall, we have shown that a simple modification of existing technology can make the types of electrodes currently used in neuroscience research suitable for use in conjunction with optogenetic methods to allow temporally and spatially precise modulation of the activity of defined neuronal subtypes in vivo to be combined with highly parallel electrical recordings.

4. Data Analysis Methods

Classically, the method employed in neuroscience to analyze the spectral contact of neural signal was Fourier analysis. Although simple and useful, basic Fourier methods suffer from a steep tradeoff between frequency and time resolution, making it unsuitable for the analysis of the rapidly-varying, interacting rhythmic patterns seen in vivo (e.g. (Tort, Kramer et al. 2008)).

However, in the last two decades three additional methods have started gaining more widespread adoption: multi-taper Fourier analysis, Hilbert analysis and wavelet methods(Le Van Quyen, Foucher et al. 2001). Although all three can be theoretically reduced to each other, practically they offer substantially different properties. While multi-taper spectral methods, such as the routines of the Chronux suite (www.chronux.org) are best suited to the analysis of relatively long recordings, Hilbert-based methods offer very good temporal and spectral resolution (Figure 1).
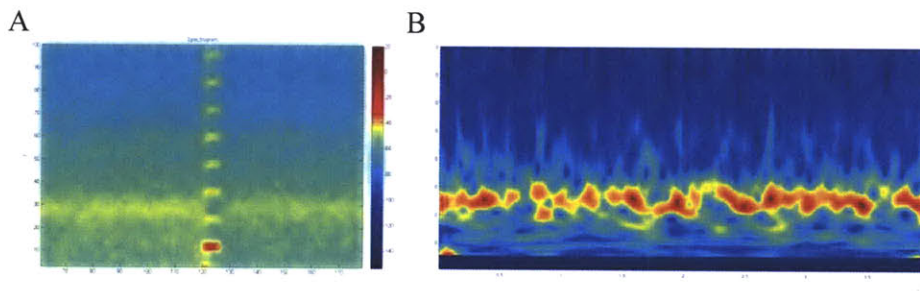
Figure 1 Extracellular recordings from a hippocampal slice bathed with 400 nM KA oscillating at gamma frequency. at t = 1.05 seconds, a train of stimuli at 12 hz was delivered. A. Time-frequency decomposition of the entire trace with the Chronux suite B. Fine-grained Hilbert analysis of a 5 second section of the trace

In addition to the absolute power and peak frequency of the oscillations, it is interesting to look at the spectral dispersion (Figure 2), as how tightly focused the rhythm may profoundly impact its biophysical and computational properties. Moreover, several perturbation paradigms can selectively affect spectral spread, without affecting other aspects of the oscillation. As a metric, we have used the width of the power spectrum at 0.67 of the peak power.
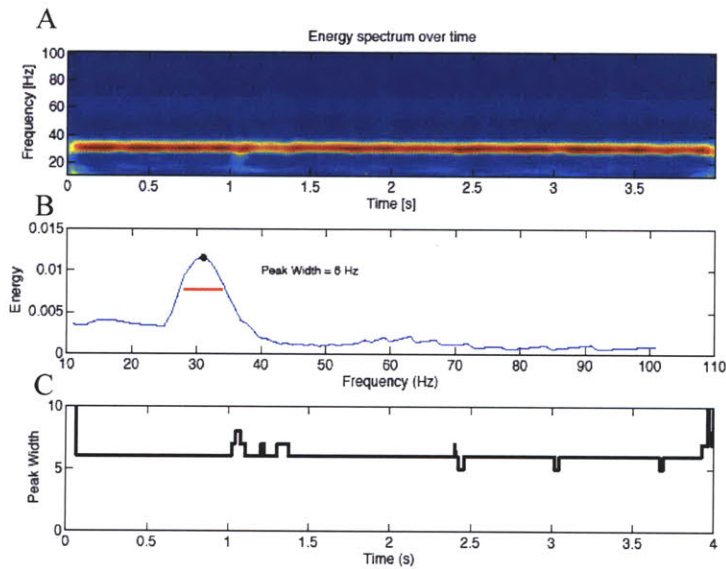
Figure 2. A. Spectral spread estimation. the top panel shows the evolution of the spectral energy content of the recorded LFP over time. A higher intensity band is clearly visible at ~30 Hz. **B.** Time-averaged energy content of frequencies 1-100 Hz. Although the peak frequency is 31 Hz, there is considerable energy in nearby frequencies. One way to quantify this phenomenon is to calculate the spectral width between the lower and upper frequencies with an energy content of 0.67 the peak. We can call that measure peak width. **C.** Plot of peak width, as previously defined, over time. It is remarkably steady in the unperturbed state, but tends to increase at the time of stimulation (100ms , low intensity pulse) at time = 1.05s.

One of the most intriguing possibilities offered by optogenetic control of neural synchrony is the ability to modulate its fine timing, e.g. synchronizing two separate oscillators, without affecting its overall power or frequency. To analyze this effect, we introduced a new metric, developed in collaboration with Adriano Tort, PhD, the inter-trial coherence (ITC) (Figures 3,4) . In essence, it provides a way to estimate how "aligned", or phase-locked, two oscillations are. For example, consider two sets of ten sinusoidal signals, either with no phase lag across them or with randomly distributed phase lags. The phase for each of the ten traces and at each time point is plotted in the unit circle. The red line represents the mean vector at each time point (mean(exp(i*φ)), where φ = [$\varphi 1$, ..., $\varphi 10$] is the vector with the ten angles). The length of this vector is the measure, i.e., ITC=abs(mean(exp(i* φ))). Note then that if all phase points are dispersed along the circle, this will provide a small mean vector (Figure 4B). Whereas if all points were exactly the same, the magnitude of the mean vector would be one (hence this measure varies from 0 to 1). For non stimulus phase-locked trials, $ITC \rightarrow 0$ with increasing the number of trials analyzed
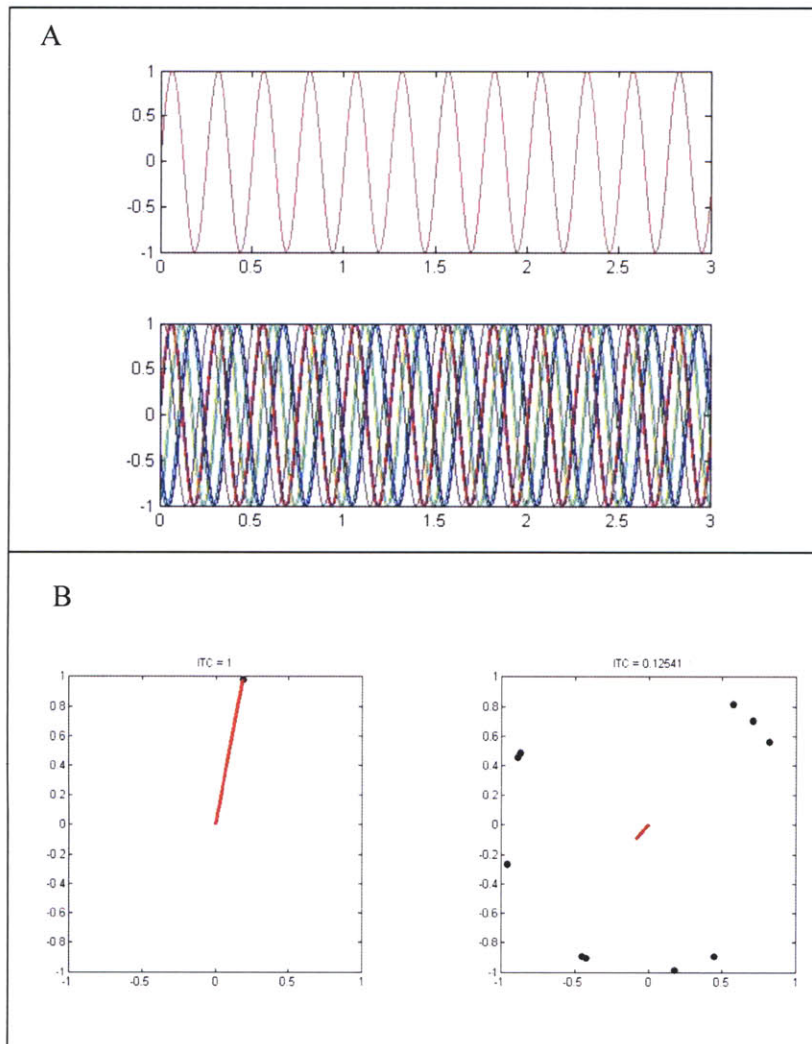
Fig. 3: Inter-trial coherence (ITC) for two sets of 10 sinusoidal signals, with either 0 or randomly distributed phase offsets. A. Raw signals. B Plot of the phases of the signals at an arbitrary time point, and the resulting ITC value.

This measure was, for example, employed in studying the phase-reset of ongoing gamma oscillations in a hippocampal slice following a brief optical stimulation of pyramidal cells (Figure 4).
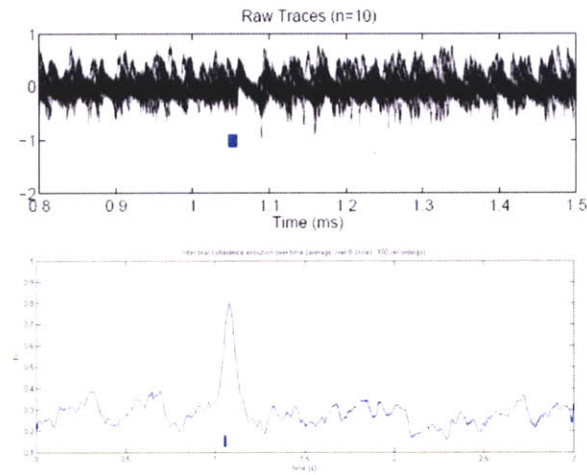
Figure 4: Example of phase-reset following a single pulse. A. Overlay of 10 traces B. ITC of population data from phase-reset experiments. In all experiments (n = 160) a 10ms pulse was delivered at t=1.05 s. The effective phase reset can be seen in the ITC peak of approximately 0.83, compared to an overall average of 0.24

A fundamental limitation of current studies of neural synchrony lies in the difficulty of establishing causal links across, for example, brain structures. It is straightforward to assess the coherence, or lack thereof, in the recordings between two regions, but it is usually not possible to distinguish which region, if any, is driving the other. To try to overcome it, we rely on two approaches: using computational methods to analyze the directionality of information flow, and closed-loop active interventions.

A number of approaches for determining the directionality of information flow have been proposed: among the most common ones are Granger Causality, Dynamic Bayesian Network analysis and the Phase-slope index.(Kaminski, Ding et al. 2001; Chen, Bressler et al. 2006; Marinazzo, Pellicoro et al. 2006; Nolte, Ziehe et al. 2008; Nedungadi, Rangarajan et al. 2009; Zou and Feng 2009).

A B
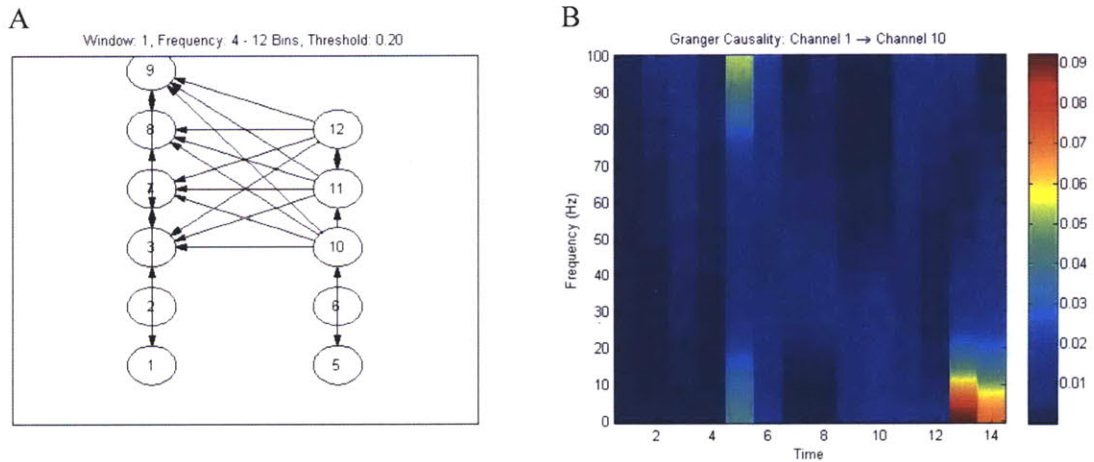
Figure 5. A. Granger causality links across recording sites. The arrows indicate the existence of a significant information transfer between the two areas, in the direction indicated by the arrow. Note that the lack of connection doesn't imply that there is no information transfer, but just that a judgment could not be made. B. Evolution of Granger causality values over time for a single pair of recording sites.

Although our experimental work has so far focused on a single region in vitro (the hippocampal CA3), we have started developing custom programs based on Granger causality using multi-electrode in vivo data from the Graybiel Lab as a sample set (Figure 5).

Closed loop control is also in its development stages, and extensive experimental application is yet lacking. The overall architecture, in its current implementation, streams data being recorded from a Digidata 1440 (Axon Instruments) to a PC, where it is processed by a custom-written software. After analysis, a stimulus paradigm is selected and sent back to the Digidata, which in turn controls a DG-4 high-speed filer changer (Leica, Germany). In order to be able to predict the trajectory of the oscillation and hence perturb it at a desired phase, the following strategy is followed (Figure 6). First, after filtering to isolate the frequency of interest (e.g. 25-35hz) we extract the instantaneous phase from the signal using Hilbert transforms. Then, plotting the oscillation in phase-time space, we pick the last recorded time point and a previous time point: a linear fit is then used to extract the slope of the phase change over time, and that is used to predict the future course of the oscillation Using closely spaced time points, just a few ms away we are able to accurately predict the phase evolution over one to three gamma cycles (depending on the level of precision desired and the stability of the oscillation).
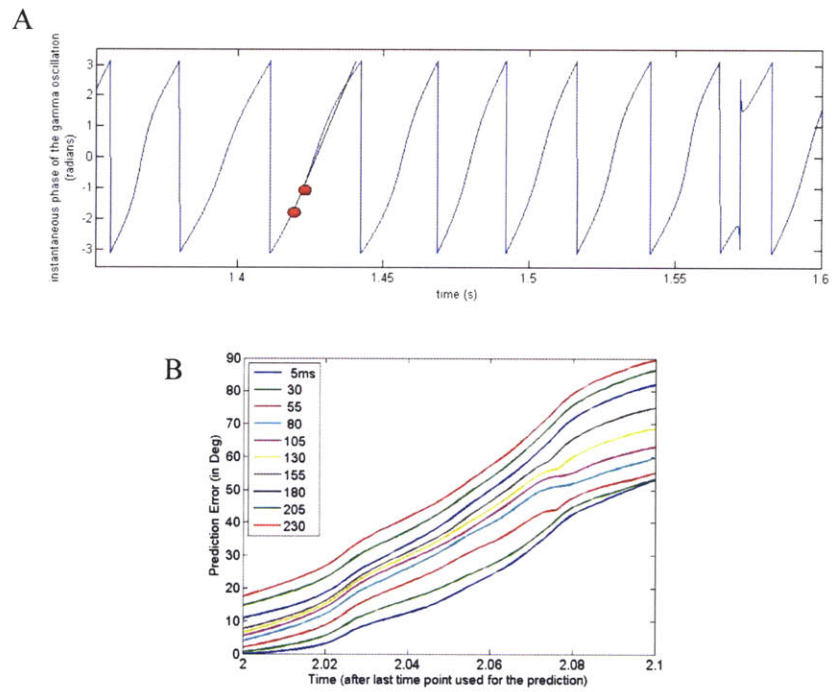
Figure 6. A. Sample phase-time trace for a gamma oscillation recording, with the two timepoints used for pase-slope estimation highlighted in red. B. Due to fluctuations in the instantaneous frequency of the oscillation, this approach allows very precise predictions up to one-three gamma cycles away, but breaks down for longer time intervals. For the same reason, using small time windows for the estimation is advantageous.

24

5. In vitro models of gamma oscillations

5.1 Introduction to in vitro slice models of gamma oscillations

Since their inception (Whittington, Traub et al. 1995; Traub, Whittington et al. 1996; Fisahn, Pike et al. 1998), slice models of neural oscillations have proved an extremely fruitful technique for beginning to unravel the fine details behind neural synchrony, with much finer resolution than currently possible in vivo. The study of γ oscillations in the hippocampal slice model, in particular, has been extensively studied. Although all oscillations in the 30-80Hz range tend to be classified as gamma, the biophysical mechanisms that bring them about, and likely their functional implications, vary substantially. Four major in vitro models of hippocampal γ have so far been studied:

5.2 Spontaneous oscillations

Most simply, oscillations may occur spontaneously, in normal artificial cerebrospinal fluid (ACSF).

5.3 "Background" gamma

Drugs may be puffed (pressure ejected) onto the tissue or introduced into the bath. Drugs used for this purpose include activators of metabotropic glutamate and kainate receptors, as well as muscarinic receptors. In this paradigm, other subtypes of receptors (including AMPA/kainate, NMDA, and GABAB) might be pharmacologically blocked. In recordings from CA1 and CA3 this protocol tends to robustly produce persistent 30-40 Hz . It is important to note, however, that although the recorded LFP induced by stimulation of muscarinic or cholinergic receptors is essentially indistinguishable, the underlying mechanism is very different, as can be evinced from pharmacological studies(Bartos, Vida et al. 2007).

5.4 Tetanic stimulation

Brief tetanic stimulation stimulation activates neurons (including axons and presynaptic terminals) directly and, additionally, leads to release of neuroactive substances (glutamate, GABA, acetylcholine, etc.). It is the neuroactive substances that induce the oscillation after a pause (about 100 ms), and the, relatively short-lasting, oscillation is not time-locked to the electrical stimulation. It can also be combined with surgical disruption of intrahippocampal pathways. The tetanic paradigm can be applied to two tissue sites at once and therefore is valuable for the study of oscillatory synchronizationbetween two sites.

5.5 "Puff" gamma

The ionic milieu can also be altered, either via changing bath ionic composition (for instance, removing calcium ions), or by pressure ejection of hypertonic solutions (for instance, hypertonic K+ solution). To some extent, the ejection of hypertonic K+ solution overlaps the tetanic paradigm, in that such a solution is expected to depolarize at least some neurons (including axons) and to release neuroactive substances such as GABA

6. Computational models of gamma rhythms

Network models have played a pivotal role in understanding the physical principles involved in in vitro oscillations and in generating experimentally testable predictions. One depends on an accurate model for grasping how an oscillation occurs at all, and how particular structural features of the network determine the frequency and number of cells participating on each wave; one can also see, in simulations, how phase relations between different neuronal types arise. This is particularly true when dealing with a large number of interacting effects (glutamatergic and gabaergic transmission; synaptic and gap-junction mediated communication) and spatially disperse networks (as the biological system always is)

One approach has been (Traub, Schmitz et al. 1999; Traub, Contreras et al. 2005) to use models with a number of cells on the order of the number present in the physical system, each modeled as a multi-compartment neuron, with a number of ion channels (extracted from the experimental literature) varying from neuron type to neuron type. Although even such a complex model is a drastic simplification of the biological system, it can capture a rich repertoire of observed phenomena, and can be used as a base for developing much simpler models (e.g. (Ermentrout & Kopell 1998, Kopell et al. 2000)), which not only are more amenable to mathematical analysis, but importantly can be more intuitively understood and manipulated, while at the same time retaining the ability to reproduce the particular behavior under study.

Although the study of different cortical areas (e.g. mEC, auditory cortex) has revealed the existence of several other gamma-generating mechanisms, the three main models employed to describe hippocampal gamma (o which we'll be focusing) are: Interneuron Network Gamma (ING), Pyramidal cell Interneuron Network Gamma (PING), and "weak" gamma.

6.1 Interneuronal Network Gamma (ING).

In all hippocampal gamma oscillations interneurons (INs) play a prominent role in shaping the rhythmic activity of the network; indeed the first model described is in fact purely interneuron-driven. Gamma oscillations in the CA1 region of the hippocampus can be induced in vitro by the

application of muscarinic agonists, even during the blockade of ionotropic excitatory postsynaptic potentials((Wang and Buzsaki 1996)). This type of gamma rhythm, called ING, does not depend on the participation of E-cells, and individual I-cells fire at or near gamma frequency(Wang and Buzsaki 1996; Chow, White et al. 1998; White, Chow et al. 1998; Tiesinga and Jose 2000), the main relevant parameters being the inhibition time constant and the firing period. ING is fragile, in the sense that coherence is usually lost when a modest amount of heterogeneity in the drives to the I-cells is introduced (Wang and Buzsaki 1996; White, Chow et al. 1998). Tiesinga and Jose' (Tiesinga and Jose 2000) have described a more robust ING-like rhythm in which there are stochastic fluctuations in the drive to the I-cells, and individual I-cells do not participate on every population cycle. Additionally, gap junctions between interneurons may help, to some degree, to compensate for inhomogeneities in drive, as seen experimentally. Although E-cells are not needed for ING, a population of E-cells may be entrained by a population of I-cells firing rhythmically and in synchrony.

6.2 Pyramidal-Interneuronal Network Gamma (PING)

A purely interneuronal network, though useful, represents a somewhat artificial abstraction from the mechanisms that can be expected to mediate γ synchrony in vivo. To take into account the ubiquitous presence of pyramidal cells another model of γ has been proposed (PING), relying on the mutual interaction of E and I cells to achieve synchronization at the network level(Kopell, Ermentrout et al. 2000; Whittington, Traub et al. 2000; Borgers and Kopell 2003)

Biophysically realistic simulations allow one to explore how variations in external drives can create or abolish PING rhythms. If drive to the I-cells becomes too strong or if drive to the E-cells becomes too weak, the PING mechanism fails: either the I-cells synchronize at too high a frequency to be entrained by the E-cells (phase walkthrough) or the I-cells do not synchronize, and their activity leads to the suppression of the E-cells, thereby removing the mechanism that could create a synchronous rhythm. In the parameter regime in which phase walkthrough occurs, no PING rhythm is possible. However, there is a region of bistability in parameter space within which both suppression of the E-cells by asynchronous activity of the I-cells and PING are possible

6.3 "Weak" gamma

In another type of gamma rhythm, the E-cells spike irregularly and at a mean frequency much below that of the population rhythm. The persistent hippocampal and neocortical gamma oscillations described above are of this type. Such rhythm has been usually called "weak" γ, to distinguish it from "strong" gamma, in which E cells fire at nearly every cycle.

One possible mechanism through which this may come about is a PING-like rhythm in which the E-cells receive randomly fluctuating drive and gamma-frequency oscillations are generated by the following mechanism: synaptic inhibition from a population spike of the I-cells abruptly halts spiking of the E-cells. As the inhibition decays, the most depolarized of the stochastically driven E-cells begin to reach threshold and spike again. The resulting volley of E-cell spikes quickly triggers a new I-cell population spike, which again halts E-cell spiking, initiating the next cycle.

Another possible mechanism is an ING rhythm in which the E-cells receive randomly fluctuating inhibitory input from the I-cells, rather than randomly fluctuating external input; computationally, this can be accomplished by giving the I-cells noisy external drive and making the I $\rightarrow$ E connection sparse and random.

6.4 The model employed in our work

The model network, which consists of 160 excitatory (E) cells, was modeled as in Olufsen et al, J. Comput. Neurosci. 2003(Olufsen, Whittington et al. 2003) and 40 inhibitory (I) cells, modeled as in Wang & Buzsáki, J. Neurosci. 1996 with (E-I,I-I, I-E) sparse, random connections. Connection strength is indicated by the thickness of the arrows. As described in Börgers, Epstein, & Kopell, PNAS 2005, stochastic drive to the E cells produces gamma oscillations. Optical stimulation was modeled as deterministic drive to a subset of cells(Borgers and Kopell 2003; Borgers and Kopell 2005).
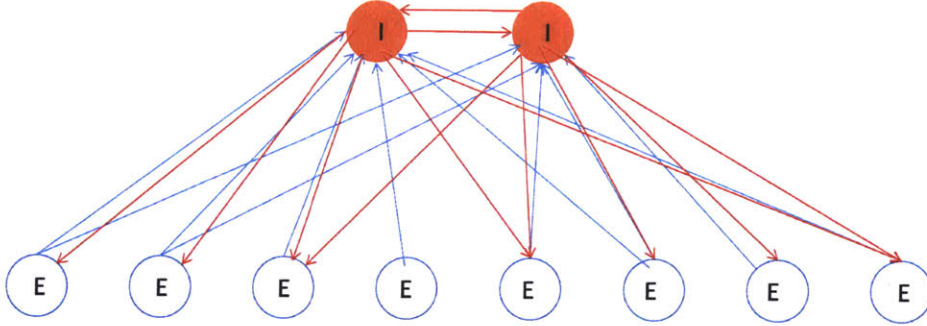
Figure 1: Model network, which consists of 160 excitatory (E) cells, modeled as in Olufsen et al, J. Comput. Neurosci. 2003 and 40 inhibitory (I) cells, modeled as in Wang & Buzsáki, J. Neurosci. 1996 with (E-I,I-I, I-E) sparse, random connections. Connection strength is indicated by the thickness of the arrows. As described in Börgers, Epstein, & Kopell, PNAS 2005, stochastic drive to the E cells produces gamma oscillations. Optical stimulation was modeled as deterministic drive to a subset of cells.

The E cells' voltage satisfied the equation:

$$\frac{CdV}{dt} = g_{Na}m^3h(V_{Na} - V) + g_K n^4(V_K - V) + g_L(V_L - V) + I \ .$$

The letters C, V, t, g, and I denote capacitance density, voltage, time, conductance density, and current density, respectively. The units used for these quantities are μF/cm2, ms, mV, mS/cm2, and μA/cm2, respectively. For brevity, units will often be omitted from here on. The parameter values are C = 1, g_{Na} = 100, V_{Na} = 50, g_K = 80, V_K = −100, g_L = 0.1, and V_L = −67, as in (Bichot, Rossi et al. 2005). The sodium activation variable m is assumed to be a function of voltage:

$$m = m\infty(V) = \frac{a_m(V)}{a_m(V) + b_m(V)} .$$

The gating variables n and h satisfy:

$$\frac{dx}{dt} = a_x(V)(1 - x) - b_x(V)x, \qquad (x = n, h)$$

30

We define a_x and b_x ($x = m,n$) :

$$a_m(V) = 0.32(V + 54)/[1 - exp(-(V + 54)/4)], b_m(V)$$

$$= 0.28(V + 27)/[exp((V + 27)/5) - 1], a_n(V)$$

$$= 0.032(V + 52)/[1 - exp(-(V + 52)/5)], b_n(V$$

$$= 0.5exp(-(V + 57)/40),$$

$$a_h(V) = 0.128exp(-(V + 50)/18), b_h(V) = 4/[1 + exp(-(V + 27)/5)]$$

The I-cells are modeled by equations of the same form. However, following
Wang and Buzsaki (Wang and Buzsaki 1996) the parameter values are now :

$$C = 1, g_{Na} = 35, V_{Na} = 55, g_K = 9, VK = -90, g_L = 0.1, and\ V_L = -65, and\ a_m(V)$$

$$= \frac{0.1(V + 35)}{\left[1 - exp\left(-\frac{V + 35}{10}\right)\right]}, b_m(V) = 4exp\left(-\frac{V + 60}{18}\right), a_n(V)$$

$$= \frac{0.05(V + 34)}{\left[1 - exp\left(-\frac{V + 34}{10}\right)\right]}, b_n(V) = 0.625exp\left(-\frac{V + 44}{80}\right), a_h(V)$$

$$= 0.35exp\left(-\frac{V + 58}{20}\right), and\ b_h(V) = \frac{5}{\left[1 + exp\left(-\frac{V + 28}{10}\right)\right]}.$$

We consider networks of N_E E-cells and N_I I-cells, with N_E = 160 and N_I = 40.

We included models of synaptic connections mediated by AMPA receptors (E→I), and GABA$_A$
receptors (I→E and I→I).

GABA$_A$ synapses are modeled by a term of the form:

$$(g/N_I) = \sum si\ j(t)\left(V_I - V_j\right)$$

on the right-hand side of the equation governing the membrane potential of cell j, where $V_I =$ -80, g = g_{IE} if cell j is excitatory, g = g_{II} if cell j in inhibitory, and the sum extends over the indices i of the I-cells. The gating variables s = s_{ij} satisfy:

$$\frac{ds}{dt} = \frac{1 + tanh\left(\frac{V_{pre}}{10}\right)}{2} * \frac{1-s}{\tau_R} - \frac{s}{\tau_D}\tau_D$$

with $t_R = 0.5$, $t_D = 10$, and V_{pre} = membrane potential of the pre-synaptic (i-th) cell. This models inhibition from fast-spiking interneurons, believed to be important for generating gamma rhythms. The term $\frac{1 + tanh\left(\frac{Vpre}{10}\right)}{2}$ can be thought of as a normalized neurotransmitter concentration. Similarly, AMPA-receptor mediated input to the I-cells is modeled by a term of the form:

$$\left(\frac{g}{N_E}\right)\sum s_{ij}(t)*V_E - V_j$$

on the right-hand side of the equation governing the membrane potential of the j-th I-cell, where $V_E = 0$, g = g_{EI}, and the sum extends over the indices I of the E-cells.

At baseline, E and I cells receive tonic inputs, modeled as a Poisson stream, and gamma-frequency oscillations spontaneously emerge (Figure 2).
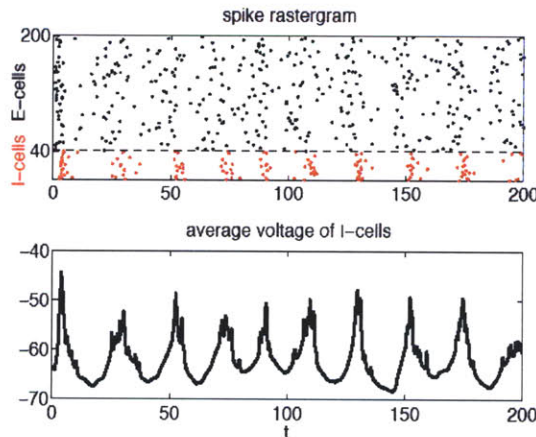
Figure 2. The model network described above spontaneously settles in gamma-frequency oscillation. Shown is a rastergram of E cells (red) and I cells (blue) spikes (top panel), and the average voltage of the I cells as a proxy for the LFP (bottom panel). Courtesy of Prof. Christoph Borgers (2009, unpublished)

Currently, a modified version of the model described above is being developed (Figure. 3), including E→E connections as well as second interneuron class, mutually connected to both E and I cells.
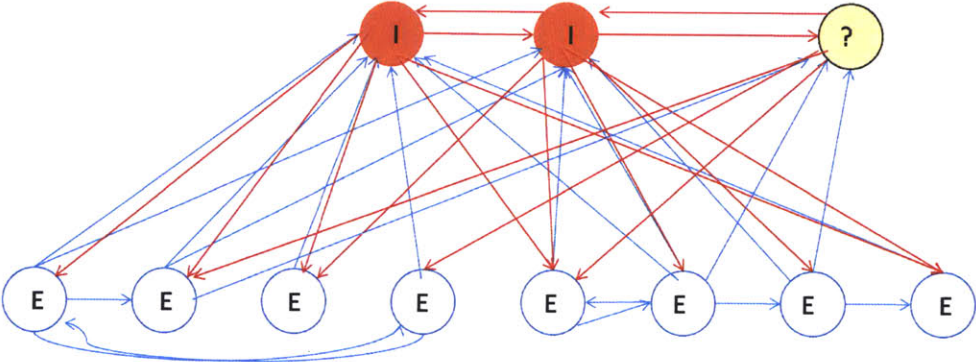
Figure 3: Current model. Sparse, random, weak E-E connections have been incorporated, as well as a second type of interneuron, reciprocally connected with E and I cells

7. Experimental methods

7.1 Virus injection in the adult mouse.

Lentiviruses were prepared as in (Boyden, Zhang et al. 2005; Bernstein, Han et al. 2008); adeno-associated viruses (AAV) were ordered from the University of Pennsylvania gene therapy vector core. Mice (PV-Cre from the Arber lab, and bred at MIT, or wild-type mice from Taconic) were anesthetized with isoflurane (1.5-2.5% in oxygen), the head shaved, and the scalp resected. With an air drill, the skull was thinned to <50 micron thickness the area of interest, and a 33 gauge needle was used to open up craniotomies. A glass micropipette filled with lentivirus or AAV, encoding for ChR2 or Halo under a cell-specific promoter or in the flip vector, and connected to a syringe pump (Harvard Apparatus), was then inserted into the brain and used to inject 1-2 microliters of virus over a 10 minute period, then let sit for 20 minutes and slowly retracted, and the incision closed. At the end of surgery, mice were given buprenorphine and meloxicam (.1 mg/kg and 1mg/kg respectively), allowed to recover, and returned to the animal facility for 1 week to allow the virus to express.

7.2 In-utero viral injections

To selectively label cortical layer 2/3 cells, we also performed in-utero virus injections. The pregnant mice (day E15.5) were anesthetized with isoflurane (1.5-2.5% in oxygen) and the abdomen shaved and cleaned. A clean midline incision was then made from the xiphoid process to the pubis, using a scalpel and iris scissors. Embryos in utero were taken out of the peritoneal cavity using sterile cotton swabs and injected in the cerebral ventricles (visualized with a strong light) with lentivirus using a Hamilton syringe tipped with a 32 gauge needle. After completing the injections, the uterus was then placed back into the peritoneal cavity and thoroughly lavaged with sterile PBS. The abdominal musculature was then sutured using 4-0 silk sutures, and the skin closed using 6-0 nylon sutures. The mouse was administered buprenorphine, recovered, and allowed to give birth normally.
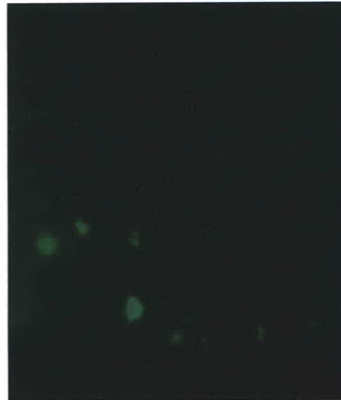
Figure 3: pyramidal neurons in layer 2-3 infected with Halo-GFP under the CamkII promoter, carried in lentivirus, injected at day 15.5

7.3 Slice preparation, recording, and oscillation induction (after(Cunningham, Hunt et al. 2006)). (Cunningham, Davies et al. 2003)

The animals employed were either of C57BL/6 background (Taconics), PV-Cre transgenic on a sv129 background (from the Arbel lab, and bred at MIT) or transgenic animals expressing Chr2-YFP under the Thy1 promoter (line 18)(Arenkiel, Peca et al. 2007).

Mice were kept under isoflurane anesthesia, and transcardially perfused with circa 20 ml of modified artificial cerebrospinal fluid (sACSF), which was composed of (in mM): Sucrose (252), KCl (3), NaH_2PO_4 (1.25), $NaHCO_3$ (24), $MgSO_4$ (2), $CaCl_2$ (2) and glucose (10). All salts were obtained from Sigma-Aldrich, USA. The brain was removed and submerged in cold (4-5 °C) sACSF during dissection, and450 m-thick horizontal slices were cut using a vibratome (Leica VT1000S, Heidelberg, Germany). Slices were then transferred to either holding chamber (at room temperature) or directly to recording chamber. Here, they were maintained at 34^0 C at the interface between a continuous stream (2 ml/min) of ACSF (composition in mM: NaCl (126), KCl (3), NaH_2PO_4 (1.25), $NaHCO_3$ (24), $MgSO_4$ (1.25), $CaCl_2$ (2) and glucose (10)), and warm, moist carbogen gas (95 % O2 : 5 % CO2). Slices were permitted to equilibrate for 45 minutes before any recordings commenced. Oscillations were induced by addition of 400 nM kainic acid (Cayman Chemicals, Inc.), or 50 µM carbachol (Sigma).

Extracellular recordings electrodes were pulled from borosilicate glass and had a final impedance of 1-3MΩ. In order to get a better sense of spatial effects some recordings were done employing voltage sensitive dyes (DI-4 anepps, Invitrogen), which, however, resulted in substantial phototoxicity and proved impractical.

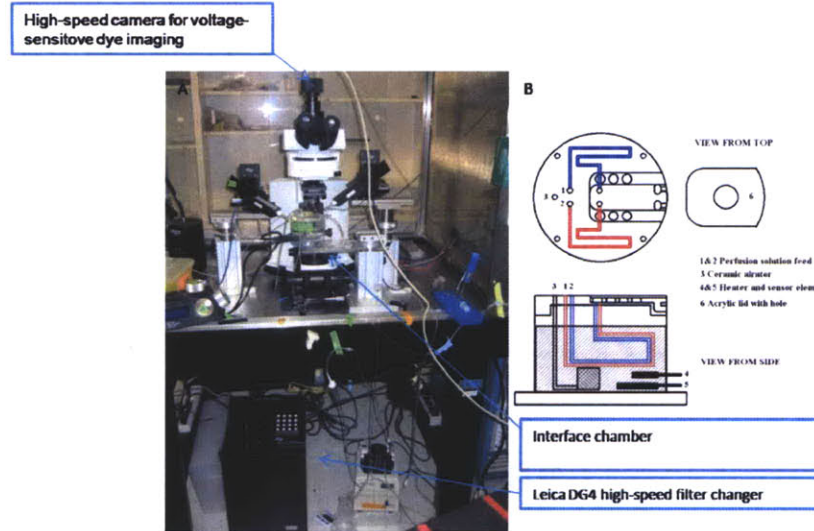**Figure 4: A. The interface-type slice rig employed for the recordings. B. Schematic of the interface chamber (Automate Scientific, CA) from www.autom8.com.**
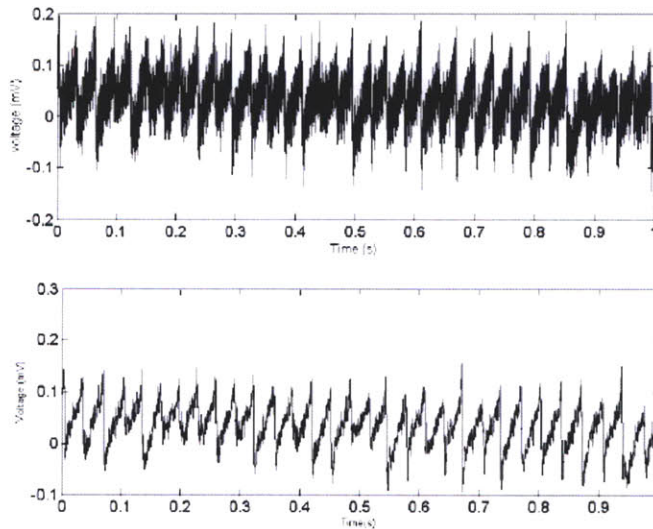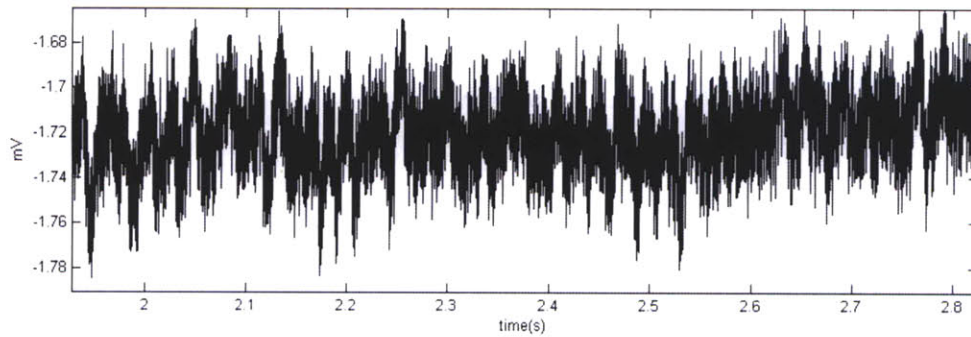

Figure 5: Gamma (30-40 Hz) oscillations induced in a hippocampal slice upon application of 400 nM kainic acid. Top: raw LFP recording. Bottom: The same recording as above, filtered between 3 and 300 Hz.

Figure 6: Raw LFP recording of beta (~25Hz) and gamma (~40-50Hz) oscillations induced in a mEC slice upon application of 400 nM kainic acid.

The recordings were carried out in the CA3 (stratum radiatum) and CA1 subfields of the hippocampus, in the Dentate Gyrus (DG) and in layers 2/3 of the medial enthorhinal cortex (mEC)

7.4 Optical perturbation.

A high-speed filter changer, Sutter DG-4 with a 300 W lamp, attached to an Olympus BX51WI was used to deliver blue (470/40x filter, Chroma) or yellow (565/50x filter, Chroma) light during the experiments. Irradiance levels employed varied between 0.1 and 100 mW/mm^2. Both pulse sequences of arbitrary complexity and continuous illumination were possible, the DG-4 being controlled with custom protocols synthesized in MATLAB and executed by the pClamp program (Molecular Devices) through the analog out ports of the Digidata acquisition device/controller (Molecular Devices).

7.5 Slice fixation, immunostaining, and cell counting.

In order to estimate the size of the cell population being driven in each experiment, we proceeded to fix, immunostain and count the number of infected cells in each slice. After recordings were completed, the slices were placed in 4% formaldehyde, between pieces of light ashless filter paper, to prevent slice curling. After fixation, they were washed and permeabilized 3 times for 30 minutes each in a solution containing PBS, 100 mM glycine, and 0.5% triton X-100 (PTG solution), and then blocked for 2 hours in a PTB solution (PTG + 2% normal goat serum from Jackson Immunochemicals). Slices were then incubated with primary antibody, in

PTB solution overnight at 4°C on a shaker, then washed 4 times for 30 minutes each with PTG solution, and then incubated in the secondary antibody in PTB solution for 2 hours at room temperature. Finally, the slices were washed 3 times for 30 minutes each with PTG solution, and for 30 minutes in PBS + 100 mM glycine. Slices were then mounted with Vectashield solution (Vector Labs), and imaged with a Zeiss LSM Pascal confocal microscope at 20x and 63x magnification (Figure 6).
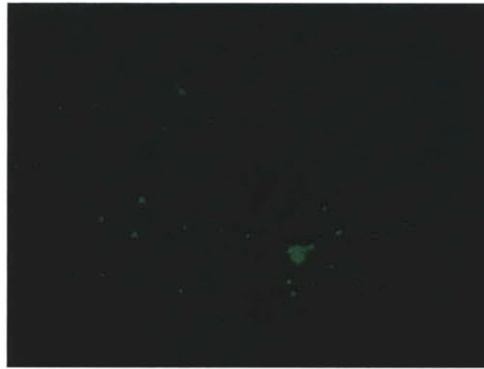
Figure 6: Confocal micrograph of a hippocampal neuron stained anti-GFP antibody

8. Experimental results and discussion.

It can be useful to think of neural rhythms at three levels of abstraction: local field potentials (the raw signal picked up by an extracellular electrode), overall behavior of different cell population (e.g. in each gamma cycle 10% of the E cells fire, and 60% of the I cells fire), and cell-assemblies, that is, the identity of the individual cells participating in the rhythm (e.g. in a network with 140 E cells, is it always the same 14 cells that fire during each gamma cycle, or are do they vary at each cycle?).

At the more "macroscopic" level, the parameters of interest are the oscillation amplitude, frequency, and phase, and those have proved relatively easy to manipulate via optogenetic methods.

Since the two main elements of this model of gamma oscillations are principal neurons and PV+ interneurons, we ideally would like to selectively drive and inhibit each class by optogenetic methods. Principal cells were either targeted via viral injections of lentivirus carrying ChIEF-GFP under the CamkII promoter or by using a transgenic line expressing Chr2-YFP under the Thy1 promoter (line 18)(Arenkiel, Peca et al. 2007). PV+ interneurons were targeted by injecting AAV viruses carrying loxP-stop-loxP-CMV- halo or loxP-stop-loxP-CMV-Chr2 into a PV-Cre transgenic line on Sv-129 background.

The early work with PV+ interneuron manipulation was only partially successful, as stimulation halo didn't seem to affect gamma (Figure 1A). Chr2, on the other hand, could as expected drive INs firing at both slow (6Hz) and high (35Hz) frequencies. (Figure 1B). Most of the work has so far been carried out on stimulation of pyramidal cells, so all the following results refer to that.
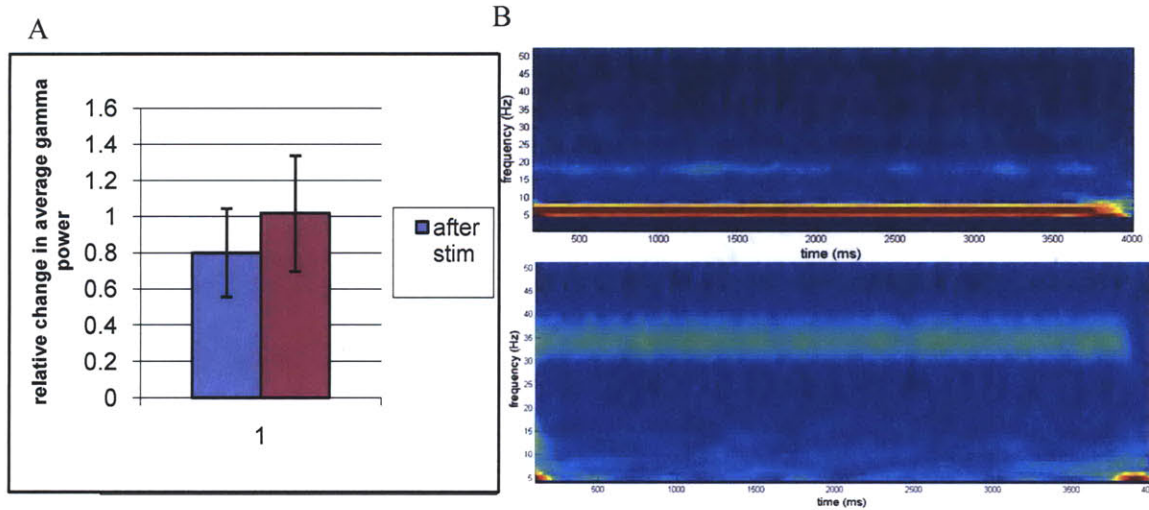
Figure 1. Experimental results modulating the activity of PV+ Ins. A. partially silencing PV+ INs with Halo is not sufficient to disrupt gamma synchrony, probably because of insufficient infection and expression levels. B. PV+ INs expressing Chr2 can be readily driven at relatively slow frequencies-in this case 6Hz (top panel) , as well as at gamma-like frequencies (35 Hz, bottom panel).

8.1 Amplitude modulation

We have explored four possible mechanisms for altering the amplitude of ongoing oscillations, each of which affects different cell populations differently, and can therefore be expected to have different functional effects, even when the overall effect on the LFP is identical.

8.1.1 Strong, rhythmic drive at the frequency of the ongoing oscillation: this is discussed in details in the section concerning frequency modulation.

8. 1.2 Long, weak drive reduces or abolishes gamma (Figure 2A,B). The decrease in gamma power is sharp but not instantaneous. The intuitive reason for this phenomenon is that the weak extra, non-synchronous (stochastic in the case of Chr2, very fast and non gamma-locked for ChIEF) drive to a subset of E cells makes the I cells not only fire more, but importantly fire more asynchronously, resulting in greatly enhanced effective inhibition, and hence disruption of gamma (Figure 2C). Recording from E cells, we should see more numerous and more "random" IPSCs, with the E cells still firing and the other E cells mostly silent, so the planned intracellular recording should help substantially in proving or disproving this hypothesis.
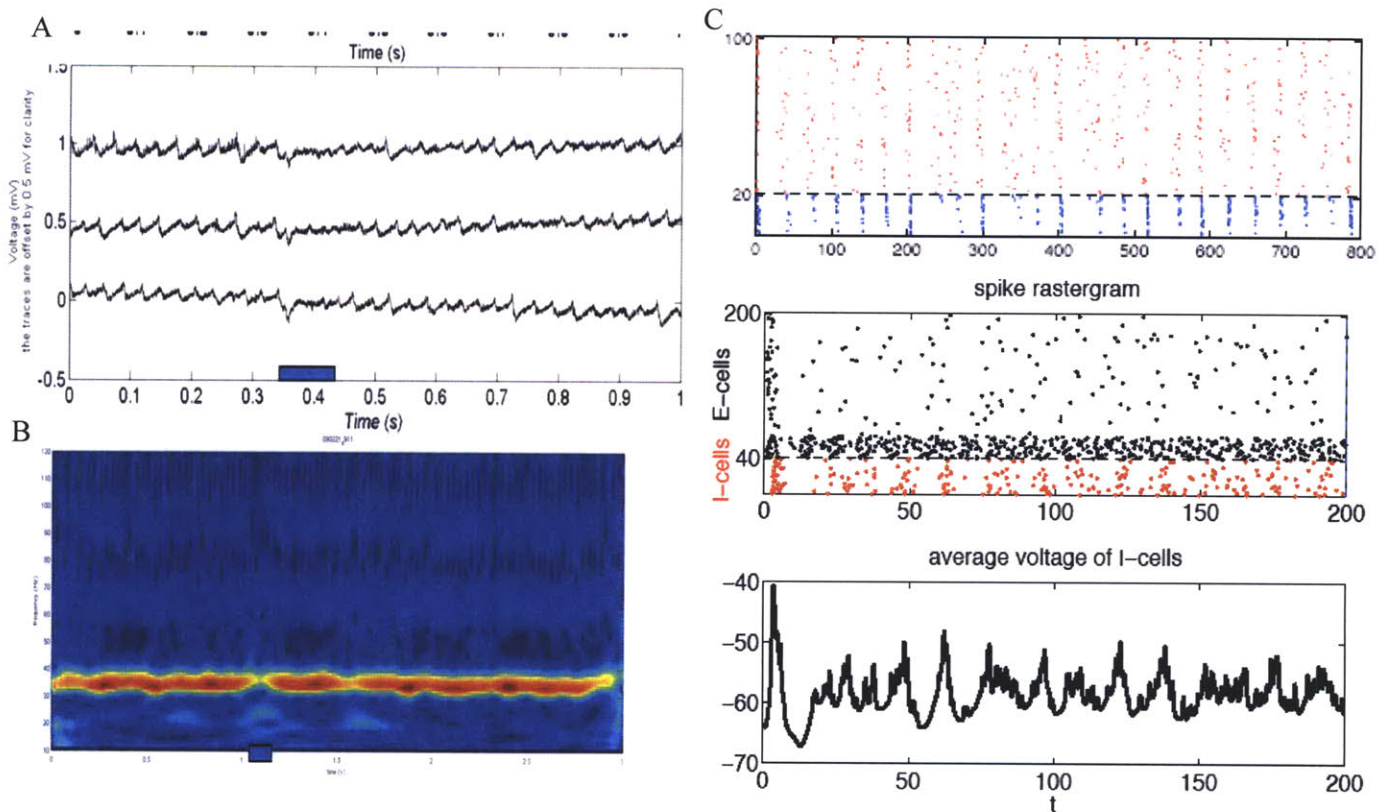
Figure 2. A. raw traces from three sequential extracellular recordings, showing reduced gamma synchrony during low-intensity stimulation with blue light. B. Averaged spectrogram from the traces above, and from seven additional trials. C. results of numerical simulations showing a spike rastergram for E and I cells during background gamma (top panel), during weak stimulation of E cells. resulting in gamma disruption (middle panel), and the average I-cells voltage (used as a proxy for the LFP). Courtesy of Prof. Christoph Börgers, unpublished.

8.1.3 Closed loop drive at different phases of the oscillation. We expect that pulses delivered at different phases of the gamma cycle may be used to either enhance or disrupt it. We have developed the hardware and software needed to implement this, and plan to carry out the experiments as soon as possible.

8.1.4 Short, strong pulse. It is also possible to use a strong, short (10 ms) pulse to induce a brief (100-250 ms) period of "silence". Note that "silence", as measured by the LFP could come about either as a result of reduced overall firing, or a desynchronization in neuronal firing, even while keeping the rate constant.

At first this result is counterintuitive, as short, brief (10ms), low intensity pulses don't affect the power of the ongoing oscillation appreciably. It may be easiest to postulate the existence of a third, important cell class that we need to include in the model. The two more reasonable candidates, based on the existing literature, are CCK+ basket cells and O-LM cells.

CCK+ basket cells are appealing because they require a stronger drive than PV+ basket cells to fire, and importantly they release GABA asynchronously(Hefft and Jonas 2005; Bartos, Vida et al. 2007). It could therefore be argued that the strong drive results in excitation of the CCK+ INs, which keep releasing GABA for the observed 100-200ms period. So while in the "long, strong" case the increased inhibition is more than compensated for by the increased drive, and the CCK+ cells quickly adapt and/or are shut down by CB1 released by the activated E cells, in this case there is no strong excitation to counteract them.

It is known that CB1 agonism reduces the power of ongoing gamma oscillations(Hajos, Katona et al. 2000; Robbe, Montgomery et al. 2006), and as CCK+ basket cells are the only HPC interneurons that express CB1Rsthis argues strongly that the effect on gamma is indeed CCK+ mediated. On the other hand, the recent work of Buzsaki and colleagues on endocannabinoids and synchrony.(Robbe, Montgomery et al. 2006), and recent physiological evidence (Katona, Urban et al. 2006; Kawamura, Fukaya et al. 2006; Takahashi and Castillo 2006) seem to indicate a possibly stronger role of CB1R's located on hippocampal pyramidal neurons.

The exact mechanism is still not completely clear, though, since cannabinoid action on pyramidal cells, if anything, leads to "release" of E cells from CCK+ INs inhibition: it is possible that the "disinhibited" E cells drive more PV+ cells, resulting in a net increase in inhibition, or at least a more asynchronous inhibition, resulting in an overall silencing of the network..

One could also maybe speculate that CCK+ INs help "sharpen" the rhythm, because they are turned off by active E cells (participating in gamma), while they keep inhibiting the other ones: a massive CB1 release would then just silence most all CCK+ cells, so that this effect is lost, resulting in decreased gamma in the LFP (but possibly increased E cells firing).

Another possible route of involvement of CCK+ INs is via $GABA_BR$, which CCK+ cells have, and which PV+ INs lack. It could then be argued that the strong E cells volley drives a massive I cells volley, and the resulting extrasynaptic GABA spillover activates $GABA_BR$ on E cells and

CCK+ cells. It is noteworthy that $GABA_B$ has been implicated in the inhibitory period seen following electrical stimulation in the cortex(Butovas, Hormuzdi et al. 2006).

This hypothesis could be tested pharmacologically, by employing selective $GABA_BR$ agonists/antagonists. An attractive alternative would be to employ optogenetic methods to silence the CCK+ cells, while driving the E cells (e.g. expressing Arch in CCK+ Ins, and ChIEF, under the control of the CamkII promoter, in pyramidal cells)

Another possible cell type to consider are O-LM cells, which are PV+, SOM+ INs. They are appealing because they have strongly facilitating synapses with E cells (Kapfer, Glickfeld et al. 2007), so that they would normally be silent, but could be recruited by a strong drive, if that resulted in a massive train of spikes. They should be easy to tell apart: their IPSCs are much slower than CCK+ and PV+, they have strong I_h currents, and they don't express either $GABA_BR$ or CB1R (and could be shut down with a SOM-Cre + flex-Arch system).

Yet another possibility (suggested by Prof. Miles Whittington) to explain the emergence of a silent period following a strong, short pulse doesn't involve the recruitment of previously-silent interneurons. The spike volley induced in the E cells by the pulse leads to substantial Ca^{++} influx which, on one hand, causes more Ca^{++}-gated K channels to open, on the other, it also affects gap junctions, which are crucial for gamma. This hypothesis could be tested by selectively blocking Ca^{++}-gated K channels, e.g. with by bath application of iberiotoxin(Kunze, Bornstein et al. 1994; Saria, Fischer et al. 2000). However, the fact that the silent period is highly stereotyped, regardless of stimulus duration may be hard to reconcile with this, as one would expect the effect to become prolonged with greater stimulation intensities and duration, which presumably lead to greater Ca^{++} influx
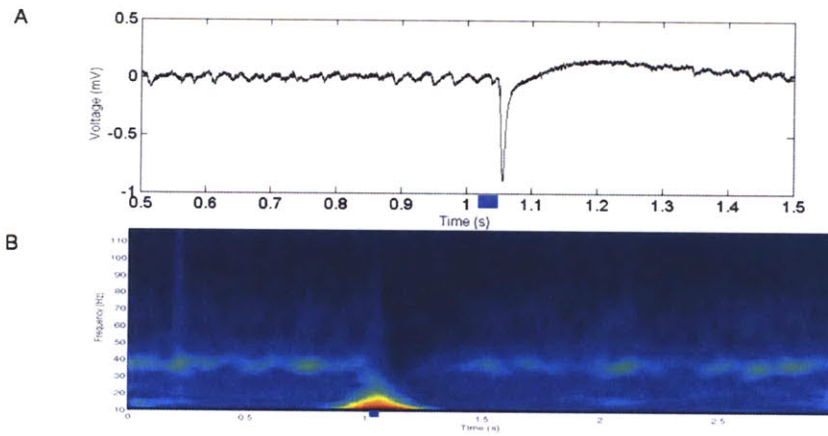
Figure 3. Representative example of the effect of a single strong 10ms pulse of blue light driving pyramidal cells in the oscillating slice, resulting in the abolition of gamma oscillations for ~200ms following stimulation. the blue bar indicates the time of stimulation. A. Raw trace of the recorded extracellular field potential. B. Energy spectrum evolution over time, averaged over ten trials
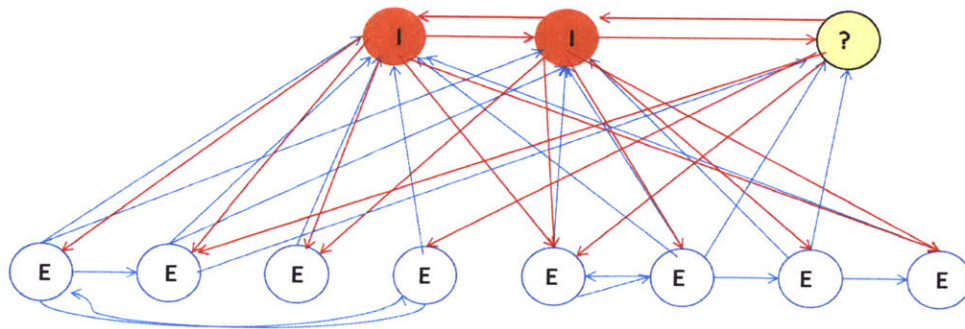
Figure 4. Simplified diagram of the current model, which includes an additional class of interneurons, connected to both I and E cells, and releasing GABA asynchronously. This addition makes the model capable of predicting the emergence of a silent period following intense stimulation

8.2 Frequency modulation

8.2.1 Strong, rhythmic drive. As one would expect, a sufficiently strong drive is able to drive the network in a wide range of frequencies, from 3 to at least 50 Hz. Note that in between the pulses, at low frequencies, there is something akin to the "silent period" described above, and similar mechanisms are likely at play.
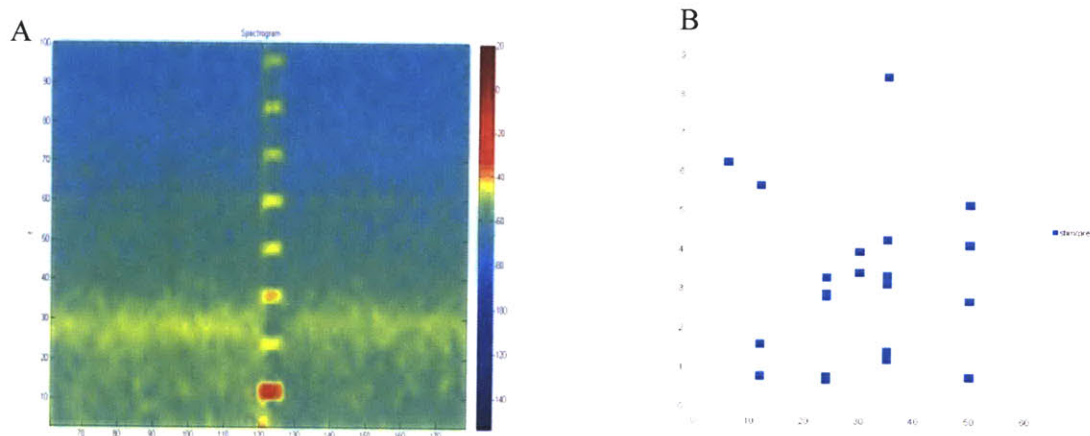
Figure 5. A. Spectrogram of ongoing gamma oscillation and strong 12 Hz stimulus train. B. For high intensity stimulation (high irradiance and/or large numbe of light-responsive cells), we failed to see a frequency dependence of the measured LFP response.

8.2.2 Long, strong pulse

By providing a strong, continuous (200ms) drive to the network, we can induce a transition from the ongoing gamma to higher frequency (50-80 Hz), precisely timed oscillations.
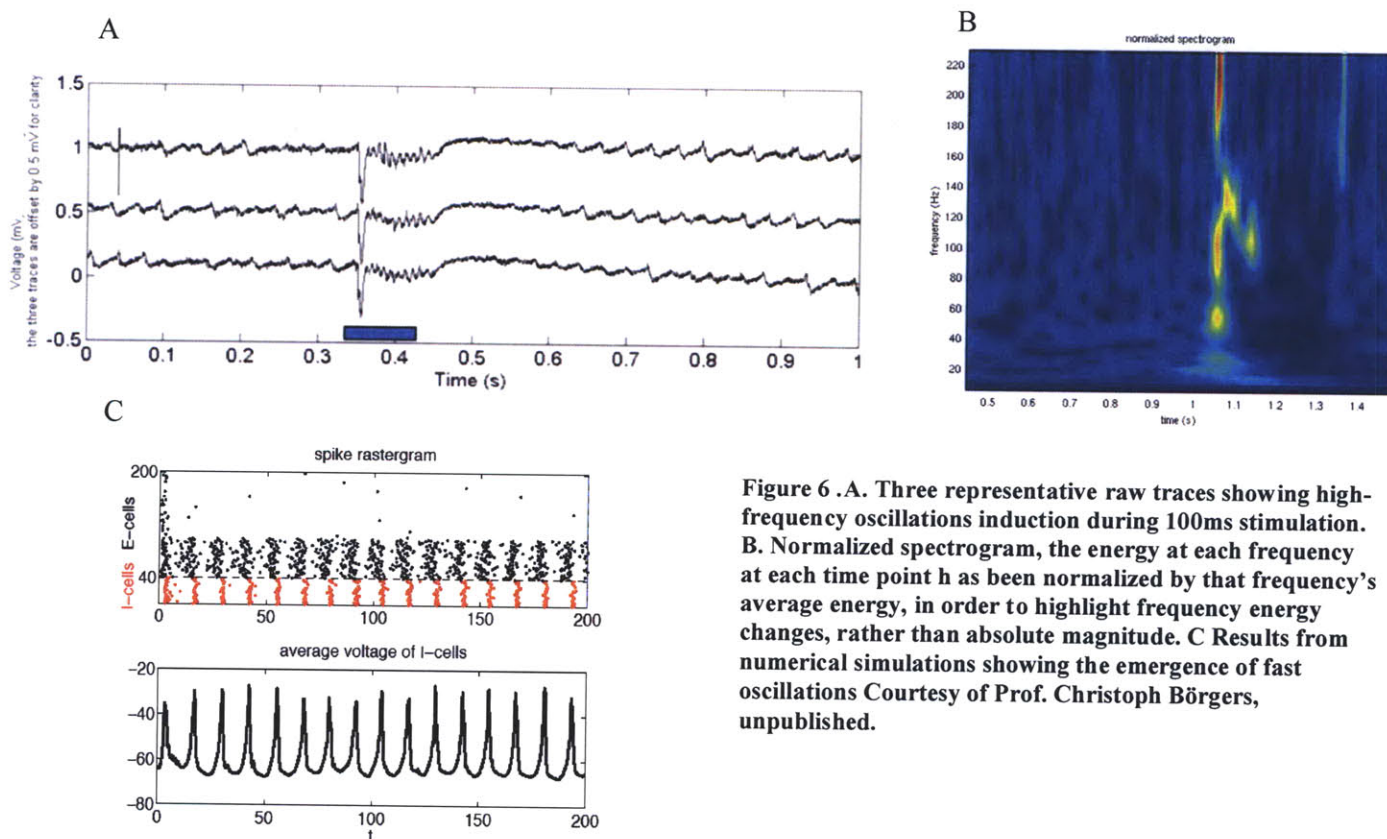
Figure 6 .A. Three representative raw traces showing high-frequency oscillations induction during 100ms stimulation. B. Normalized spectrogram, the energy at each frequency at each time point h as been normalized by that frequency's average energy, in order to highlight frequency energy changes, rather than absolute magnitude. C Results from numerical simulations showing the emergence of fast oscillations Courtesy of Prof. Christoph Börgers, unpublished.

8.2.3 Entrainment

Finally, it is possible entrain an oscillating network by delivering brief (10ms) pulses of light at the desired frequency. Some of the questions that then arise, and which we have only started to address experimentally is whether there a well-defined range of frequencies for which this is possible? Is there a specific resonant frequency for the system? Does this affect only the magnitude or also the precision and temporal carry-over of the synchronization (after the stimulation is discontinued)?

A

B
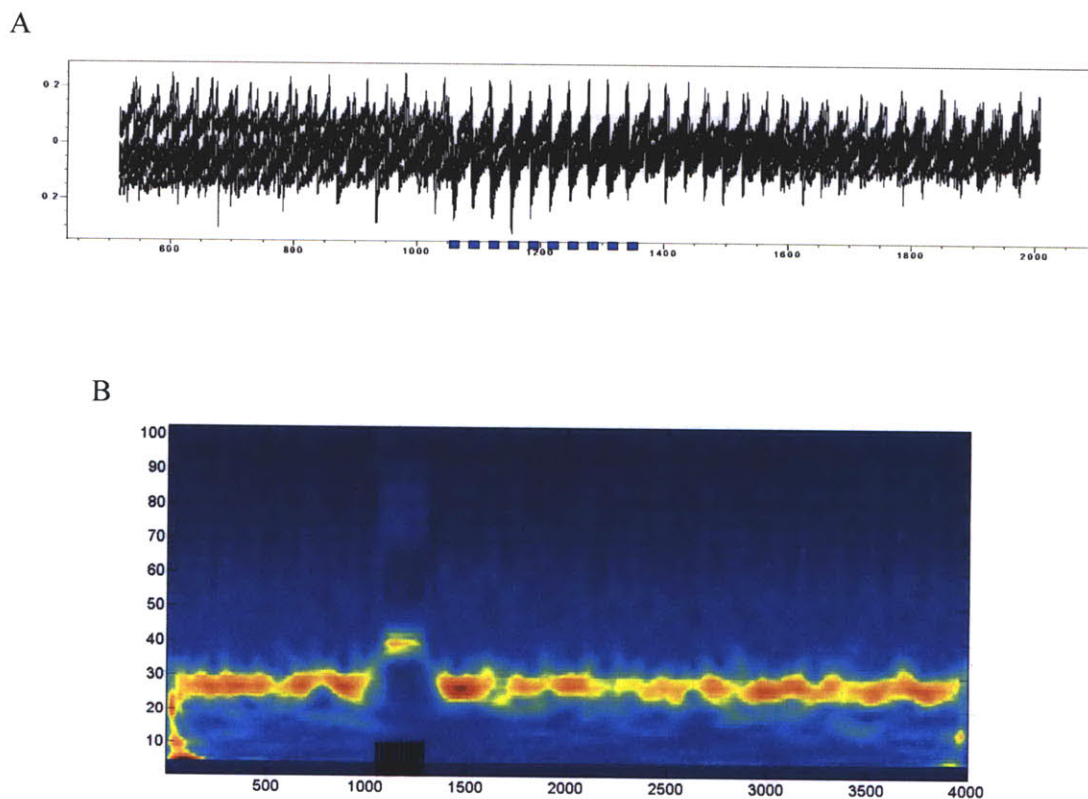
Figure 6. Entrainment of the ongoing gamma oscillation by a train of short (10ms) pulses. A. Superimposed raw traces from ten trials. The blue bars indicate the stimulation pulses, which were delivered at 31 Hz (frequency of the ongoing gamma: 30 Hz) B. The same approach can also be used to substantially shift the oscillation frequency. In this case from ~28 Hz to 40 Hz (Spectrogram, averaged over ten trials)
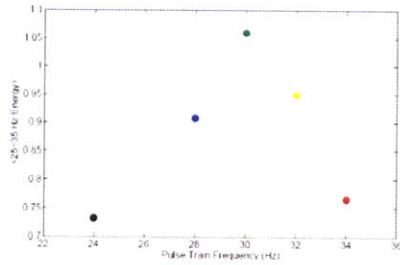
Figure 7. Possible resonance in the frequency response of the network to trains of brief pulses.
Entraining the network with trains of 10 10ms pulses at different frequencies evoked a stronger
response when they were closer to the frequency of the ongoing gamma oscillation (the network's
"natural frequency"), 30 Hz. Image courtesy of Adriano Tort, PhD.

8.3 Modulation of spectral spread. In addition to the average frequency of the ongoing gamma
oscillations, another relevant parameter, still in the frequency domain, is the spectral focus of the
oscillation: given an average frequency of, e.g. 30 Hz, is it almost perfectly uniform or does it
vary between 25 and 35Hz? Computationally, the two cases are expected to result in very
different properties. One approach to quantifying spectral spread is simply to take the width of
the spectral peak at 0.67 of its peak amplitude. This captures most all information for unimodal
distributions and when the type of distribution doesn't vary much; for more complex cases, an
approach we have pursued is to fit the data with more complex functions, extracting two relevant
parameters. There is, however, as we increase the number of free parameters, there is a tradeoff
between how much information is captured and how easily interpretable in terms of the
underlying physiology the result is. In the limit, by using as many parameters as data points we
can fit the results perfectly, but we wouldn't have gained any insight.
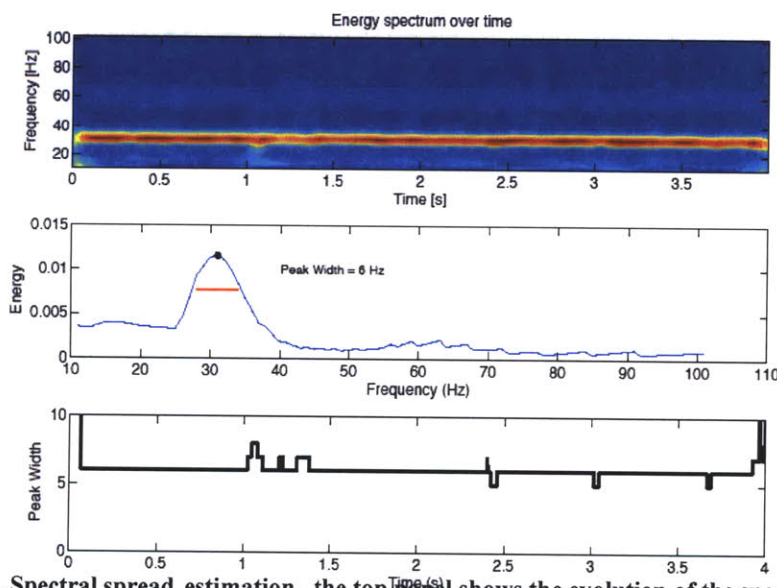
Figure 8. A. Spectral spread estimation. the top panel shows the evolution of the spectral energy content of the recorded LFP over
time. A higher intensity band is clearly visible at ~30 Hz. **B.** Time-averaged energy content of frequencies 1-100 Hz. Although the
peak frequency is 31Hz, there is considerable energy in nearby frequencies. One way to quantify this phenomenon is to calculate
the spectral width between the lower and upper frequencies with an energy content of 0.67 the peak. We can call that measure
peak width. **C.** Plot of peak width, as previously defined, over time. It is remarkably steady in the unperturbed state, but tends to
increase at the time of stimulation (100ms, low intensity pulse) at time = 1.05s.

8.4 Phase reset.

Phase reset of ongoing oscillations has been correlated to cognitive and sensory activity(Howard, Rizzuto et al. 2003; Rizzuto, Madsen et al. 2003; McCartney, Johnson et al. 2004; Mormann, Fell et al. 2005; Crane, Windels et al. 2009), and many functions of gamma are postulated to rely on its phase. It would therefore be advantageous to be able to selectively affect the phase of an oscillation in a controllable fashion without altering its other properties. From the model we described, we would expect that this could be brought about by inducing a volley of E cells firing, which in turn drives a synchronized volley from the I cells, effectively resetting the network(Borgers and Kopell 2003)(Figure 7), without necessarily altering overall amplitude. Experimentally, this is indeed the case (Figures 8,9).
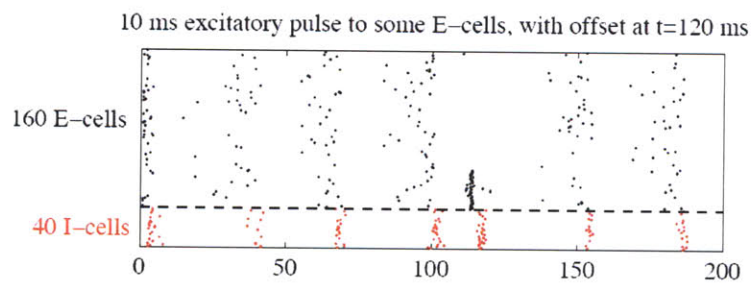
Figure 7. Results of numerical simulations (rastergram) suggesting that a single driving pulse to E cells may be able to effectively phase-reset the ongoing oscillation. Courtesy of Prof. Christoph Börgers, unpublished.
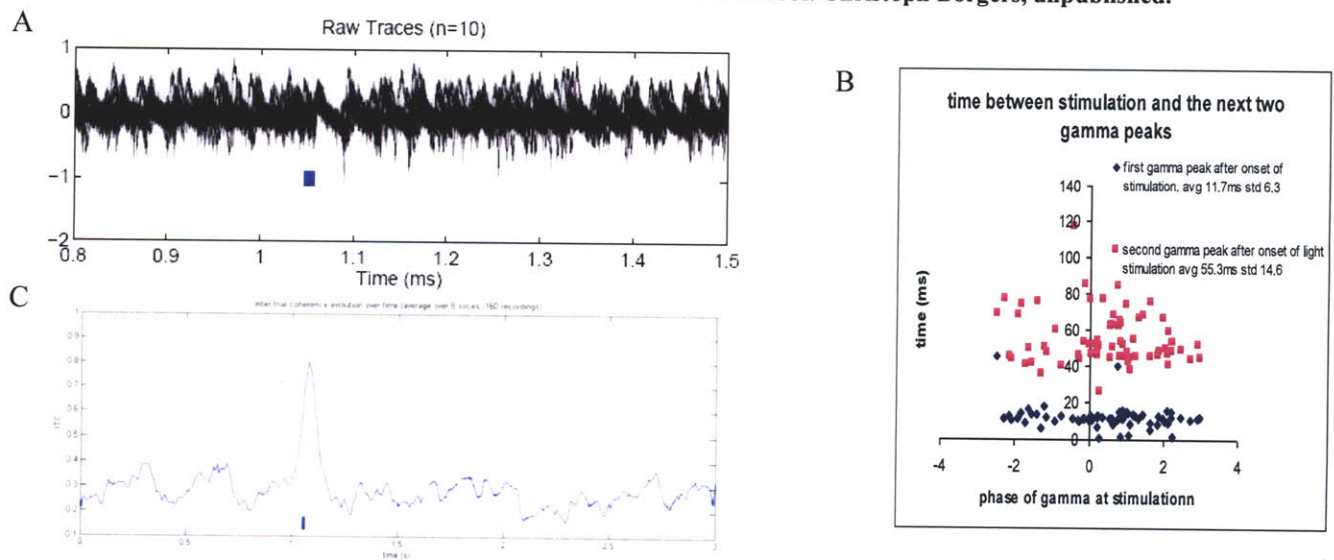
Figure 8 Experimental results showing phase-reset of ongoing oscillations following a 10ms pulse of moderate (1-5mW/mm^2) intensity. A. Superimposed traces from ten trials. The blue bar indicates the time of stimulation. B. Time interval between the light offset and the next two peaks of the oscillation, showing no dependence on the phase of the oscillation at the time of stimulation. C ITC plot for 160 trials, showing massive synchronization induced by the stimulus pulse (0.83, compared to 0.24 baseline).
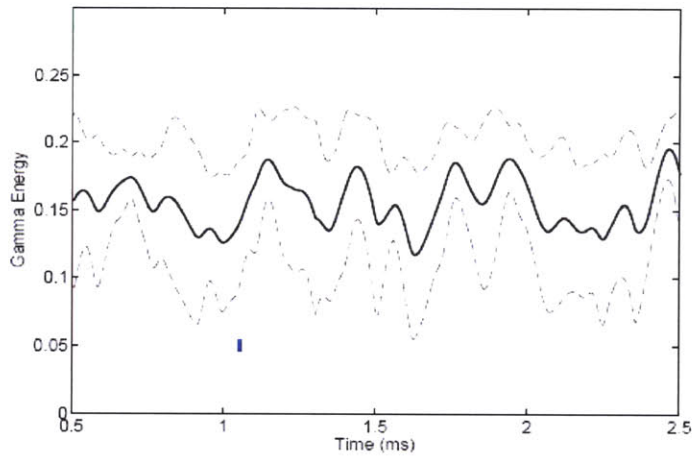
Figure 9. Plot of gamma energy over time (mean +-s.d.) for the same ten trials as in Figure 8A. The stimulation (indicated by the blue bar, at t = 1.05s) has no discernible effect on it.

9. Conclusions and a look forward

We have successfully employed optogenetic techniques to modulate neural synchrony with much finer control than previously possible. Simultaneously, we have worked with our collaborators toward progressively refining a system that remained as simple as possible, while still being able not only to reproduce the main experimental findings, but importantly to guide the development of new modulation paradigms and predicting its effects almost at a very fine, cell-assembly level, something which is currently not possible experimentally.

The next steps for the very near term will be to perform single-cell recordings during the stimulation paradigms described in section 8.0, in order to verify that our mechanistic understanding of what is happening, as detailed by the model, is indeed correct. Similarly, pharmacological blockade or stimulation of CB1Rs and $GABA_BRs$ should further help clarify the mechanism behind the emergence of a silent period following a strong drive to the E cells population. Understanding this in detail could prove particularly interesting as this phenomenon appears to place clear boundaries to the size of a cell assembly that can be active at the same time in the same network, at least in a given situation. It is likely that different types of oscillations or behavioral states in vivo can modulate this phenomenon, and it may be worthwhile to try modulating it via optogenetic methods, but all of this is postulated on a specific mechanism.

Although single-cell and whole-cell recordings will prove crucial to validating our models and our interpretation of the experimental results, the models will then allow us to predict the behavior of cell populations on a very fine scale, in response to a variety of manipulations, in manner that is vastly more efficient than trying to map out each effect experimentally. This aspect will prove even more important as we move to systems that are either less characterized or more difficult to interrogate experimentally (e.g. in vivo). In developing suitable models for new targets, we will be able to build upon the considerable wealth of work that has been carried out on modeling the emergence of synchronous behavior in various regions with in vitro preparations(Cunningham, Hunt et al. 2006; Middleton, Jalics et al. 2008; Roopun, Cunningham et al. 2008; Roopun, Kramer et al. 2008).

We expect that the ability to control the frequency and/or the phase of the ongoing oscillation with only minimal perturbation to its other parameters will prove extremely useful in testing experimentally some of the proposed theories concerning the role of synchrony in neural function. For example, whether there are indeed region-specific "resonant frequencies" that help information transfer, what is the role of gamma phase and cell assemblies in the encoding and retrieving of items stored in working memory, or whether disrupting or enhancing synchrony across regions showing ongoing oscillations during a behavioral task can impair or enhance performance, both in "normal" animals and in animal models of disease characterized by aberrations in neural rhythms.

Of course, this will almost certainly not be as simple as, e.g. driving vast numbers of Chr2-expressing E cells with 40 Hz trains of stimuli to "address" the decreased gamma-band oscillations in schizophrenia. Rather, the use of optogenetic tools, in conjunction with models allowing the prediction of the effect of stimulation upon distinct cell assemblies and cell populations could in many cases allow the use of specific stimulation paradigms (possibly operating in a feedback fashion in a closed-loop control system such as we have developed) to restore the network to a more normal pattern of fine-scale activity.

Indeed, this work has also highlighted some of the subtleties of dealing with neural synchrony, inasmuch as it is often an emergent property of a complex system, rather than something imposed externally, which can be arbitrarily changed without affecting any other aspect of the system. However, a combination of targeted optogenetic methods and suitable computational modeling should allow for the first time a causal assessment of the functions and mechanics of neural synchrony

10. References

Arenkiel, B. R., J. Peca, et al. (2007). "In vivo light-induced activation of neural circuitry in transgenic mice expressing channelrhodopsin-2." Neuron 54(2): 205-18.

Bartos, M., I. Vida, et al. (2007). "Synaptic mechanisms of synchronized gamma oscillations in inhibitory interneuron networks." Nat Rev Neurosci 8(1): 45-56.

Borgers, C. and N. Kopell (2003). "Synchronization in networks of excitatory and inhibitory neurons with sparse, random connectivity." Neural Comput 15(3): 509-38.

Crane, J. W., F. Windels, et al. (2009). "Oscillations in the basolateral amygdala: aversive stimulation is state dependent and resets the oscillatory phase." J Neurophysiol.

Hajos, N., I. Katona, et al. (2000). "Cannabinoids inhibit hippocampal GABAergic transmission and network oscillations." Eur J Neurosci 12(9): 3239-49.

Hefft, S. and P. Jonas (2005). "Asynchronous GABA release generates long-lasting inhibition at a hippocampal interneuron-principal neuron synapse." Nat Neurosci 8(10): 1319-28.

Howard, M. W., D. S. Rizzuto, et al. (2003). "Gamma oscillations correlate with working memory load in humans." Cereb Cortex 13(12): 1369-74.

Kapfer, C., L. L. Glickfeld, et al. (2007). "Supralinear increase of recurrent inhibition during sparse activity in the somatosensory cortex." Nat Neurosci 10(6): 743-53.

Katona, I., G. M. Urban, et al. (2006). "Molecular composition of the endocannabinoid system at glutamatergic synapses." J Neurosci 26(21): 5628-37.

Kawamura, Y., M. Fukaya, et al. (2006). "The CB1 cannabinoid receptor is the major cannabinoid receptor at excitatory presynaptic sites in the hippocampus and cerebellum." J Neurosci 26(11): 2991-3001.

Kunze, W. A., J. C. Bornstein, et al. (1994). "Charybdotoxin and iberiotoxin but not apamin abolish the slow after-hyperpolarization in myenteric plexus neurons." Pflugers Arch 428(3-4): 300-6.

McCartney, H., A. D. Johnson, et al. (2004). "Theta reset produces optimal conditions for long-term potentiation." Hippocampus 14(6): 684-7.

Mormann, F., J. Fell, et al. (2005). "Phase/amplitude reset and theta-gamma interaction in the human medial temporal lobe during a continuous word recognition memory task." Hippocampus 15(7): 890-900.

Rizzuto, D. S., J. R. Madsen, et al. (2003). "Reset of human neocortical oscillations during a working memory task." Proc Natl Acad Sci U S A 100(13): 7931-6.

Robbe, D., S. M. Montgomery, et al. (2006). "Cannabinoids reveal importance of spike timing coordination in hippocampal function." Nat Neurosci 9(12): 1526-33.

Saria, A., H. S. Fischer, et al. (2000). "Margatoxin and iberiotoxin, two selective potassium channel inhibitors, induce c-fos like protein and mRNA in rat organotypic dorsal striatal slices." Amino Acids 19(1): 23-31.

Takahashi, K. A. and P. E. Castillo (2006). "The CB1 cannabinoid receptor mediates glutamatergic synaptic suppression in the hippocampus." Neuroscience 139(3): 795-802.

Borgers, C., S. Epstein, et al. (2005). "Background gamma rhythmicity and attention in cortical local circuits: a computational study." Proc Natl Acad Sci U S A 102(19): 7002-7.

Borgers, C., S. Epstein, et al. (2008). "Gamma oscillations mediate stimulus competition and attentional selection in a cortical network model." Proc Natl Acad Sci U S A 105(46): 18023-8.

Fries, P., D. Nikolic, et al. (2007). "The gamma cycle." Trends Neurosci 30(7): 309-16.

Gray, C. M., P. Konig, et al. (1989). "Oscillatory responses in cat visual cortex exhibit inter-columnar synchronization which reflects global stimulus properties." Nature 338(6213): 334-7.

Jensen, O., J. Kaiser, et al. (2007). "Human gamma-frequency oscillations associated with attention and memory." Trends Neurosci 30(7): 317-24.

Kopell, N., G. B. Ermentrout, et al. (2000). "Gamma rhythms and beta rhythms have different synchronization properties." Proc Natl Acad Sci U S A 97(4): 1867-72.

Singer, W. (1999). "Neuronal synchrony: a versatile code for the definition of relations?" Neuron 24(1): 49-65, 111-25.

Tort, A. B., H. G. Rotstein, et al. (2007). "On the formation of gamma-coherent cell assemblies by oriens lacunosum-moleculare interneurons in the hippocampus." Proc Natl Acad Sci U S A 104(33): 13490-5.

Uhlhaas, P. J., D. E. Linden, et al. (2006). "Dysfunctional long-range coordination of neural activity during Gestalt perception in schizophrenia." J Neurosci 26(31): 8168-75.

Adamantidis, A. R., F. Zhang, et al. (2007). "Neural substrates of awakening probed with optogenetic control of hypocretin neurons." Nature 450(7168): 420-4.

Atasoy, D., Y. Aponte, et al. (2008). "A FLEX switch targets Channelrhodopsin-2 to multiple cell types for imaging and long-range circuit mapping." J Neurosci 28(28): 7025-30.

Bernstein, J. G., X. Han, et al. (2008). "Prosthetic systems for therapeutic optical activation and silencing of genetically-targeted neurons." Proc Soc Photo Opt Instrum Eng 6854: 68540H.

Boyden, E. S., F. Zhang, et al. (2005). "Millisecond-timescale, genetically targeted optical control of neural activity." Nat Neurosci 8(9): 1263-8.

Furler, S., J. C. Paterna, et al. (2001). "Recombinant AAV vectors containing the foot and mouth disease virus 2A sequence confer efficient bicistronic gene expression in cultured cells and rat substantia nigra neurons." Gene Ther 8(11): 864-73.

Han, X. and E. S. Boyden (2007). "Multiple-color optical activation, silencing, and desynchronization of neural activity, with single-spike temporal resolution." PLoS One 2(3): e299.

Han, X., X. Qian, et al. (2009). "Millisecond-timescale optical control of neural dynamics in the nonhuman primate brain." Neuron 62(2): 191-8.

Kuhlman, S. J. and Z. J. Huang (2008). "High-resolution labeling and functional manipulation of specific neuron types in mouse brain by Cre-activated viral gene expression." PLoS One 3(4): e2005.

Lagali, P. S., D. Balya, et al. (2008). "Light-activated channels targeted to ON bipolar cells restore visual function in retinal degeneration." Nat Neurosci 11(6): 667-75.

Lin, J. Y., M. Z. Lin, et al. (2009). "Characterization of engineered channelrhodopsin variants with improved properties and kinetics." Biophys J 96(5): 1803-14.

Nagel, G., M. Brauner, et al. (2005). "Light activation of channelrhodopsin-2 in excitable cells of Caenorhabditis elegans triggers rapid behavioral responses." Curr Biol 15(24): 2279-84.

Petreanu, L., D. Huber, et al. (2007). "Channelrhodopsin-2-assisted circuit mapping of long-range callosal projections." Nat Neurosci 10(5): 663-8.

Schroll, C., T. Riemensperger, et al. (2006). "Light-induced activation of distinct modulatory neurons triggers appetitive or aversive learning in Drosophila larvae." Curr Biol 16(17): 1741-7.

Wang, H., J. Peca, et al. (2007). "High-speed mapping of synaptic connectivity using photostimulation in Channelrhodopsin-2 transgenic mice." Proc Natl Acad Sci U S A 104(19): 8143-8.

Wang, H., Y. Sugiyama, et al. (2009). "Molecular determinants differentiating photocurrent properties of two channelrhodopsins from chlamydomonas." J Biol Chem 284(9): 5685-96.

Zhang, F., A. M. Aravanis, et al. (2007). "Circuit-breakers: optical technologies for probing neural signals and systems." Nat Rev Neurosci 8(8): 577-81.

Zhang, F., M. Prigge, et al. (2008). "Red-shifted optogenetic excitation: a tool for fast neural control derived from Volvox carteri." Nat Neurosci 11(6): 631-3.

Zhang, Y. P. and T. G. Oertner (2007). "Optical induction of synaptic plasticity using a light-sensitive channel." Nat Methods 4(2): 139-41.

Bernstein, J. G., X. Han, et al. (2008). "Prosthetic systems for therapeutic optical activation and silencing of genetically-targeted neurons." Proc Soc Photo Opt Instrum Eng 6854: 68540H.

Buzsaki, G. (2004). "Large-scale recording of neuronal ensembles." Nat Neurosci 7(5): 446-51.

Gratzel, M. (2001). "Photoelectrochemical cells." Nature 414(6861): 338-344.

Han, X., X. Qian, et al. (2009). "Millisecond-timescale optical control of neural dynamics in the nonhuman primate brain." Neuron 62(2): 191-8.

Honda, K. (2004). "Dawn of the evolution of photoelectrochemistry." Journal of Photochemistry and Photobiology A: Chemistry 166(1-3): 63-68.

Kipke, D. R., W. Shain, et al. (2008). "Advanced neurotechnologies for chronic neural interfaces: new horizons and clinical opportunities." J Neurosci 28(46): 11830-8.

Adamantidis, A. R., F. Zhang, et al. (2007). "Neural substrates of awakening probed with optogenetic control of hypocretin neurons." Nature 450(7168): 420-4.

Arenkiel, B. R., J. Peca, et al. (2007). "In vivo light-induced activation of neural circuitry in transgenic mice expressing channelrhodopsin-2." Neuron 54(2): 205-18.

Atasoy, D., Y. Aponte, et al. (2008). "A FLEX switch targets Channelrhodopsin-2 to multiple cell types for imaging and long-range circuit mapping." J Neurosci 28(28): 7025-30.

Bartos, M., I. Vida, et al. (2007). "Synaptic mechanisms of synchronized gamma oscillations in inhibitory interneuron networks." Nat Rev Neurosci 8(1): 45-56.

Bernstein, J. G., X. Han, et al. (2008). "Prosthetic systems for therapeutic optical activation and silencing of genetically-targeted neurons." Proc Soc Photo Opt Instrum Eng 6854: 68540H.

Bichot, N. P., A. F. Rossi, et al. (2005). "Parallel and serial neural mechanisms for visual search in macaque area V4." Science 308(5721): 529-34.

Borgers, C., S. Epstein, et al. (2005). "Background gamma rhythmicity and attention in cortical local circuits: a computational study." Proc Natl Acad Sci U S A 102(19): 7002-7.

Borgers, C., S. Epstein, et al. (2008). "Gamma oscillations mediate stimulus competition and attentional selection in a cortical network model." Proc Natl Acad Sci U S A 105(46): 18023-8.

Borgers, C. and N. Kopell (2003). "Synchronization in networks of excitatory and inhibitory neurons with sparse, random connectivity." Neural Comput 15(3): 509-38.

Borgers, C. and N. Kopell (2005). "Effects of noisy drive on rhythms in networks of excitatory and inhibitory neurons." Neural Comput 17(3): 557-608.

Boyden, E. S., F. Zhang, et al. (2005). "Millisecond-timescale, genetically targeted optical control of neural activity." Nat Neurosci 8(9): 1263-8.

Butovas, S., S. G. Hormuzdi, et al. (2006). "Effects of electrically coupled inhibitory networks on local neuronal responses to intracortical microstimulation." J Neurophysiol 96(3): 1227-36.

Buzsaki, G. (2004). "Large-scale recording of neuronal ensembles." Nat Neurosci 7(5): 446-51.

Chen, Y., S. L. Bressler, et al. (2006). "Stochastic modeling of neurobiological time series: power, coherence, Granger causality, and separation of evoked responses from ongoing activity." Chaos 16(2): 026113.

Chow, C. C., J. A. White, et al. (1998). "Frequency control in synchronized networks of inhibitory neurons." J Comput Neurosci 5(4): 407-20.

Crane, J. W., F. Windels, et al. (2009). "Oscillations in the basolateral amygdala: aversive stimulation is state dependent and resets the oscillatory phase." J Neurophysiol.

Cunningham, M. O., C. H. Davies, et al. (2003). "Gamma oscillations induced by kainate receptor activation in the entorhinal cortex in vitro." J Neurosci 23(30): 9761-9.

Cunningham, M. O., J. Hunt, et al. (2006). "Region-specific reduction in entorhinal gamma oscillations and parvalbumin-immunoreactive neurons in animal models of psychiatric illness." J Neurosci 26(10): 2767-76.

Fisahn, A., F. G. Pike, et al. (1998). "Cholinergic induction of network oscillations at 40 Hz in the hippocampus in vitro." Nature 394(6689): 186-9.

Fries, P., D. Nikolic, et al. (2007). "The gamma cycle." Trends Neurosci 30(7): 309-16.

Furler, S., J. C. Paterna, et al. (2001). "Recombinant AAV vectors containing the foot and mouth disease virus 2A sequence confer efficient bicistronic gene expression in cultured cells and rat substantia nigra neurons." Gene Ther 8(11): 864-73.

Gratzel, M. (2001). "Photoelectrochemical cells." Nature 414(6861): 338-344.

Gray, C. M., P. Konig, et al. (1989). "Oscillatory responses in cat visual cortex exhibit inter-columnar synchronization which reflects global stimulus properties." Nature 338(6213): 334-7.

Hajos, N., I. Katona, et al. (2000). "Cannabinoids inhibit hippocampal GABAergic transmission and network oscillations." Eur J Neurosci 12(9): 3239-49.

Han, X. and E. S. Boyden (2007). "Multiple-color optical activation, silencing, and desynchronization of neural activity, with single-spike temporal resolution." PLoS One 2(3): e299.

Han, X., X. Qian, et al. (2009). "Millisecond-timescale optical control of neural dynamics in the nonhuman primate brain." Neuron 62(2): 191-8.

Hefft, S. and P. Jonas (2005). "Asynchronous GABA release generates long-lasting inhibition at a hippocampal interneuron-principal neuron synapse." Nat Neurosci 8(10): 1319-28.

Honda, K. (2004). "Dawn of the evolution of photoelectrochemistry." Journal of Photochemistry and Photobiology A: Chemistry 166(1-3): 63-68.

Howard, M. W., D. S. Rizzuto, et al. (2003). "Gamma oscillations correlate with working memory load in humans." Cereb Cortex 13(12): 1369-74.

Jensen, O., J. Kaiser, et al. (2007). "Human gamma-frequency oscillations associated with attention and memory." Trends Neurosci 30(7): 317-24.

Kaminski, M., M. Ding, et al. (2001). "Evaluating causal relations in neural systems: granger causality, directed transfer function and statistical assessment of significance." Biol Cybern 85(2): 145-57.

Kapfer, C., L. L. Glickfeld, et al. (2007). "Supralinear increase of recurrent inhibition during sparse activity in the somatosensory cortex." Nat Neurosci 10(6): 743-53.

Katona, I., G. M. Urban, et al. (2006). "Molecular composition of the endocannabinoid system at glutamatergic synapses." J Neurosci 26(21): 5628-37.

Kawamura, Y., M. Fukaya, et al. (2006). "The CB1 cannabinoid receptor is the major cannabinoid receptor at excitatory presynaptic sites in the hippocampus and cerebellum." J Neurosci 26(11): 2991-3001.

Kipke, D. R., W. Shain, et al. (2008). "Advanced neurotechnologies for chronic neural interfaces: new horizons and clinical opportunities." J Neurosci 28(46): 11830-8.

Kopell, N., G. B. Ermentrout, et al. (2000). "Gamma rhythms and beta rhythms have different synchronization properties." Proc Natl Acad Sci U S A 97(4): 1867-72.

Kuhlman, S. J. and Z. J. Huang (2008). "High-resolution labeling and functional manipulation of specific neuron types in mouse brain by Cre-activated viral gene expression." PLoS One 3(4): e2005.

Kunze, W. A., J. C. Bornstein, et al. (1994). "Charybdotoxin and iberiotoxin but not apamin abolish the slow after-hyperpolarization in myenteric plexus neurons." Pflugers Arch 428(3-4): 300-6.

Lagali, P. S., D. Balya, et al. (2008). "Light-activated channels targeted to ON bipolar cells restore visual function in retinal degeneration." Nat Neurosci 11(6): 667-75.

Le Van Quyen, M., J. Foucher, et al. (2001). "Comparison of Hilbert transform and wavelet methods for the analysis of neuronal synchrony." J Neurosci Methods 111(2): 83-98.

Lin, J. Y., M. Z. Lin, et al. (2009). "Characterization of engineered channelrhodopsin variants with improved properties and kinetics." Biophys J 96(5): 1803-14.

Litvin, F. F., O. A. Sineshchekov, et al. (1978). "Photoreceptor electric potential in the phototaxis of the alga Haematococcus pluvialis." Nature 271(5644): 476-8.

Marinazzo, D., M. Pellicoro, et al. (2006). "Nonlinear parametric model for Granger causality of time series." Phys Rev E Stat Nonlin Soft Matter Phys 73(6 Pt 2): 066216.

McCartney, H., A. D. Johnson, et al. (2004). "Theta reset produces optimal conditions for long-term potentiation." Hippocampus 14(6): 684-7.

Middleton, S., J. Jalics, et al. (2008). "NMDA receptor-dependent switching between different gamma rhythm-generating microcircuits in entorhinal cortex." Proc Natl Acad Sci U S A 105(47): 18572-7.

Mormann, F., J. Fell, et al. (2005). "Phase/amplitude reset and theta-gamma interaction in the human medial temporal lobe during a continuous word recognition memory task." Hippocampus 15(7): 890-900.

Nagel, G., M. Brauner, et al. (2005). "Light activation of channelrhodopsin-2 in excitable cells of Caenorhabditis elegans triggers rapid behavioral responses." Curr Biol 15(24): 2279-84.

Nedungadi, A. G., G. Rangarajan, et al. (2009). "Analyzing multiple spike trains with nonparametric granger causality." J Comput Neurosci.

Nolte, G., A. Ziehe, et al. (2008). "Robustly estimating the flow direction of information in complex physical systems." Phys Rev Lett 100(23): 234101.

Olufsen, M. S., M. A. Whittington, et al. (2003). "New roles for the gamma rhythm: population tuning and preprocessing for the Beta rhythm." J Comput Neurosci 14(1): 33-54.

Petreanu, L., D. Huber, et al. (2007). "Channelrhodopsin-2-assisted circuit mapping of long-range callosal projections." Nat Neurosci 10(5): 663-8.

Rizzuto, D. S., J. R. Madsen, et al. (2003). "Reset of human neocortical oscillations during a working memory task." Proc Natl Acad Sci U S A 100(13): 7931-6.

Robbe, D., S. M. Montgomery, et al. (2006). "Cannabinoids reveal importance of spike timing coordination in hippocampal function." Nat Neurosci 9(12): 1526-33.

Roopun, A. K., M. O. Cunningham, et al. (2008). "Region-specific changes in gamma and beta2 rhythms in NMDA receptor dysfunction models of schizophrenia." Schizophr Bull 34(5): 962-73.

Roopun, A. K., M. A. Kramer, et al. (2008). "Temporal Interactions between Cortical Rhythms." Front Neurosci 2(2): 145-54.

Saria, A., H. S. Fischer, et al. (2000). "Margatoxin and iberiotoxin, two selective potassium channel inhibitors, induce c-fos like protein and mRNA in rat organotypic dorsal striatal slices." Amino Acids 19(1): 23-31.

Schroll, C., T. Riemensperger, et al. (2006). "Light-induced activation of distinct modulatory neurons triggers appetitive or aversive learning in Drosophila larvae." Curr Biol 16(17): 1741-7.

Singer, W. (1999). "Neuronal synchrony: a versatile code for the definition of relations?" Neuron 24(1): 49-65, 111-25.

Takahashi, K. A. and P. E. Castillo (2006). "The CB1 cannabinoid receptor mediates glutamatergic synaptic suppression in the hippocampus." Neuroscience 139(3): 795-802.

Tiesinga, P. H. and J. V. Jose (2000). "Robust gamma oscillations in networks of inhibitory hippocampal interneurons." Network 11(1): 1-23.

Tort, A. B., M. A. Kramer, et al. (2008). "Dynamic cross-frequency couplings of local field potential oscillations in rat striatum and hippocampus during performance of a T-maze task." Proc Natl Acad Sci U S A 105(51): 20517-22.

Tort, A. B., H. G. Rotstein, et al. (2007). "On the formation of gamma-coherent cell assemblies by oriens lacunosum-moleculare interneurons in the hippocampus." Proc Natl Acad Sci U S A 104(33): 13490-5.

Traub, R. D., D. Contreras, et al. (2005). "Single-column thalamocortical network model exhibiting gamma oscillations, sleep spindles, and epileptogenic bursts." J Neurophysiol 93(4): 2194-232.

Traub, R. D., D. Schmitz, et al. (1999). "High-frequency population oscillations are predicted to occur in hippocampal pyramidal neuronal networks interconnected by axoaxonal gap junctions." Neuroscience 92(2): 407-26.

Traub, R. D., M. A. Whittington, et al. (1996). "Analysis of gamma rhythms in the rat hippocampus in vitro and in vivo." J Physiol 493 (Pt 2): 471-84.

Uhlhaas, P. J., D. E. Linden, et al. (2006). "Dysfunctional long-range coordination of neural activity during Gestalt perception in schizophrenia." J Neurosci 26(31): 8168-75.

Wang, H., J. Peca, et al. (2007). "High-speed mapping of synaptic connectivity using photostimulation in Channelrhodopsin-2 transgenic mice." Proc Natl Acad Sci U S A 104(19): 8143-8.

Wang, H., Y. Sugiyama, et al. (2009). "Molecular determinants differentiating photocurrent properties of two channelrhodopsins from chlamydomonas." J Biol Chem 284(9): 5685-96.

Wang, X. J. and G. Buzsaki (1996). "Gamma oscillation by synaptic inhibition in a hippocampal interneuronal network model." J Neurosci 16(20): 6402-13.

White, J. A., C. C. Chow, et al. (1998). "Synchronization and oscillatory dynamics in heterogeneous, mutually inhibited neurons." J Comput Neurosci 5(1): 5-16.

Whittington, M. A., R. D. Traub, et al. (1995). "Synchronized oscillations in interneuron networks driven by metabotropic glutamate receptor activation." Nature 373(6515): 612-5.

Whittington, M. A., R. D. Traub, et al. (2000). "Inhibition-based rhythms: experimental and mathematical observations on network dynamics." Int J Psychophysiol 38(3): 315-36.

Zhang, F., A. M. Aravanis, et al. (2007). "Circuit-breakers: optical technologies for probing neural signals and systems." Nat Rev Neurosci 8(8): 577-81.

Zhang, F., M. Prigge, et al. (2008). "Red-shifted optogenetic excitation: a tool for fast neural control derived from Volvox carteri." Nat Neurosci 11(6): 631-3.

Zhang, Y. P. and T. G. Oertner (2007). "Optical induction of synaptic plasticity using a light-sensitive channel." Nat Methods 4(2): 139-41.

Zou, C. and J. Feng (2009). "Granger causality vs. dynamic Bayesian network inference: a comparative study." BMC Bioinformatics 10: 122.